UCRL-17813
c.2

University of California

Ernest O. Lawrence Radiation Laboratory

A BEAM STUDY OF $N_2^+ + H_2$, HD, D_2 REACTION DYNAMICS

W. R. Gentry

(Ph. D. Thesis)

September 1967

TWO-WEEK LOAN COPY

This is a Library Circulating Copy
which may be borrowed for two weeks.
For a personal retention copy, call
Tech. Info. Division, Ext. 5545

UCRL-17813
c.2

DISCLAIMER

This document was prepared as an account of work sponsored by the United States Government. While this document is believed to contain correct information, neither the United States Government nor any agency thereof, nor the Regents of the University of California, nor any of their employees, makes any warranty, express or implied, or assumes any legal responsibility for the accuracy, completeness, or usefulness of any information, apparatus, product, or process disclosed, or represents that its use would not infringe privately owned rights. Reference herein to any specific commercial product, process, or service by its trade name, trademark, manufacturer, or otherwise, does not necessarily constitute or imply its endorsement, recommendation, or favoring by the United States Government or any agency thereof, or the Regents of the University of California. The views and opinions of authors expressed herein do not necessarily state or reflect those of the United States Government or any agency thereof or the Regents of the University of California.

Ph. D. Thesis

UCRL-17813

UNIVERSITY OF CALIFORNIA
Lawrence Radiation Laboratory
Berkeley, California

AEC Contract No. W-7405-eng-48

A BEAM STUDY OF $N_2^+ + H_2$, HD, D_2 REACTION DYNAMICS

W. R. Gentry

(Ph. D. Thesis)

September 1967

Table of Contents

Abstract iii

I. Introduction 1

A. "Classical" Studies of Ion-Molecule Reactions 2

B. The Molecular Beam Method for Study of Reaction Dynamics.... 3

C. Summary of Previous Work on the $N_2^+ + H_2$, HD, D_2 Reactions... 6

D. The Present Experiments 9

II. Instrumentation and Operating Procedure 11

A. General Description of the Apparatus 11

B. Operating Conditions and Procedure 11

C. Factors Affecting the Accuracy of Measurements 13

III. Results 15

A. Data Analysis 15

B. Contour Maps of the Complete Product Ion Distributions..... 23

C. Energetic and Intensity Data 36

IV. Discussion and Interpretation 44

A. The Potential Energy Surface for the Reaction 44

B. Models for the Dynamics 45

1. Polarization Model 45

2. Complex Model 46

3. Stripping Model 47

4. The Rebound Mechanism 56

C. Comparison of the Experimental Results with the Models..... 56

V. Conclusions 66

References 68

Acknowledgements 70

A BEAM STUDY OF $N_2^+ + H_2$, HD, D_2 REACTION DYNAMICS

W. R. Gentry

Inorganic Materials Research Division, Lawrence Radiation Laboratory,
and Department of Chemistry, University of California,
Berkeley, California

September 1967

ABSTRACT

An ion beam-collision cell method was used to measure the product energy and angular distributions from reactions of N_2^+ with H_2, HD and D_2 in the primary ion energy range 25-135 eV. The data include three contour maps each for the H_2 and D_2 experiments (taken at low, intermediate and high energies) showing the entire distribution of product intensity in the center of mass coordinate system. The distributions have a crater-like shape around the center-of-mass point. At large scattering angles the intensity varies slowly with angle, and the velocity at the rim of the crater is independent of angle in the center-of-mass system. All of the distributions have a peak at 0° scattering angle which shows little spreading in energy or angle over the spread in the primary ion beam. The intensity of this peak is 3-500 times that for the large angle scattering. Kinematic analysis of the distributions shows that all product ions are formed with high excitation energies. The amount of transfer of kinetic energy of the reactants to excitation energy of the products is found to be ~1.75 eV for the large angle scattering, independent of the primary ion energy. For the small angle scattering the energy transfer agrees with predictions of the stripping model for collisions at low energies, but at high collision energies it reaches

a constant maximum value of ~2.5 eV. This result is interpreted as evidence for $N_2 + H^+$ as the principal dissociation products of N_2H^+. Only isolated features of the product ion distributions are found to agree with simple collision models, and at high energies strong recoil is kinematically required by the data, even for the forward scattering peaks.

I. Introduction

A. "Classical" Studies of Ion-Molecule Reactions[1]

Considering the long history of interest in the kinetics of ionic processes in solution and the great advances in the understanding of gas phase kinetics made during and prior to the 1930's*, it seems at first remarkable that systematic investigations of ion-molecule reaction kinetics in the gas phase were not undertaken until the 1950's.[2,3] The reason for this, of course, was that the experimental methods of homogeneous gas phase kinetics were simply not applicable to the study of ion-molecule reactions, since the ions were available only under non-equilibrium conditions and in relatively extremely small quantities. Consequently, until very recently practically all knowledge concerning gas phase ion-molecule reactions had come from observations on the composition of the gas in mass spectrometer ion sources. Although secondary reactions (after the primary ionization) has been known to occur ever since the very beginning of mass spectrometry†, the study of the chemistry taking place within mass spectrometer ion sources was generally confined until after 1950 to merely discovering which reactions occurred. With a typical electron bombardment ion source, these

---

* For example, transition state theory was first applied to a specific reaction in 1932.[4]

† Even J. J. Thomson, with his original mass spectroscope, noticed a product from a hydrogen discharge with mass-to-charge ratio of 3, which was later shown to be due to the reaction[3]

$$H_2^+ + H_2 \rightarrow H_3^+ + H.$$

experiments consisted of passing a mixture of gases into the source, bombarding the mixture with electrons of known energy and observing the mass spectrum. Since the threshold for creation of a given ion by electron impact is generally fairly sharp with respect to the electron energy, the primary ion responsible for a given product could often be identified by the electron energy at which the product began to appear in the spectrum. By then measuring the intensity of the secondary ion peak as a function of the partial pressures of the components of the gas mixture, individual steps in the reaction could be deduced. Variations on this method included ionization of the gas by means of photons or alpha particles.

Later developments in the understanding of the influence of ion source and extraction field geometry on the mass spectra enabled the determination of rate constants analogous to those for homogeneous gas phase reactions from the dependence of secondary ion intensity on the ion repeller voltage. These studies were begun in the middle and late 1950's by several groups of workers.[1] Another technique developed in the same period was the use of a pulsed beam of ionizing electrons through the source, followed by fast extraction of the created ions after a measured time lag.[2] This method also yields thermal rate constant data.

More recently tandem mass spectrometers for study of ion-molecule reactions have come into use. In this method the primary ions are created in a separate chamber, formed into a beam and mass analyzed. They are then passed through a cell containing the neutral molecules and the products of ion-molecule reactions in the cell analyzed with a second mass spectrometer. Ionic products of the collisions may be

quantitatively extracted and their intensities measured under the condition that little momentum is transferred to the secondary ions, in which case the ions are extracted perpendicular to the primary ion beam, or under the condition that the momentum transfer is large, in which case the secondary ions are extracted parallel to the primary beam. By varying the potential of the ion source in this arrangement, the total cross section for the process can be determined as a function of the translational energy of the primary ion and, of course, since the ion beam is mass selected, there is no ambiguity about the identity of the reactants. The conditions necessary for quantitative collection of the secondary ions, however, greatly restrict the number of systems amenable to study by this method.

It is clear that studies with conventional or tandem mass spectrometers, though valuable in discovering and characterizing some general features of ion-molecule reactions, cannot be expected to yield any direct information on the details of the dynamics of elementary processes.

B. The Molecular Beam Method for Study of Reaction Dynamics[5]

The most fundamental conceivable experiment which might be done to study the details of a bimolecular chemical reaction (barring the possibility of directly observing the atoms during the collision itself) would be to prepare the two molecules in the desired electronic, vibrational and rotational states, cause them to collide with known velocity and angle of impact, then measure the velocity, angle of deflection and internal states of the products. In fact it has been the practice of chemists since the early days of molecular theory to think

about and describe reactions in terms of models in which these parameters are known. Though it has always been presumed that chemical rearrangements are due to more or less elementary dynamical interactions between the atoms involved in the collision, and though many of the basic ideas of modern chemical kinetics have arisen from the success of models for the collisions in explaining some macroscopic properties of reactant systems, there had until very recently been no direct experimental data produced on the dynamics of even the most elementary bimolecular collision. Molecular beam methods provide, in principle at least, the means of performing such experiments.

A molecular beam (which may be a beam of ions) is defined as a directed stream of molecules moving through a vacuum. By passing a collimated beam through a toothed-wheel or other velocity selector (for an ion beam, an electric or magnetic field) then through selectors which preferentially focus molecules with the desired internal states*, the initial conditions of the molecules can in principal be selected to any degree of accuracy. If two such beams are crossed, and similar selectors used to measure the distribution of products resulting from single collisions in the intersection volume, the "ideal" experiment is very nearly achieved.

---

* For example, the rotational states of polar diatomics can be selectively focused with an electric quadrupole field, an electric six-pole field can be used to select symmetric top molecules with the same dipole moment components and rotational angular momentum orientation, and individual spin states of paramagnetic atoms and molecules can be separated by a magnetic six-pole field.[10]

The present state of molecular beam research, however, falls far short of this ideal due to the low intensities available in the primary beams and the high cost of each additional selection component in terms of intensity. Only barely emerging from infancy, molecular beam research on reactions between neutrals has so far been confined principally to alkali metal reactions with halogen-containing molecules because of the ease with which the alkali metals and their halides may be detected via surface ionization, the very large reaction cross sections, and the high pumping speed of cryogenic surfaces for these materials, which is necessary to reduce the background to manageable proportions. Even the most elementary early studies, where two thermal beams were crossed and the angular distributions of scattered products measured, yielded direct information on the kinematics of the reactions which allowed inferences to be made concerning the reaction probability as a function of the impact parameter of the collision and the relative orientation of the partners.[5] The later addition of velocity analysis in the alkali metal beam and then velocity analysis of both the alkali metal beam and the product beam has allowed very detailed study of the dynamics, including the dependence of the reaction probability on relative translational energy and the determination of the excitation energy of products as a function of scattering angle and the translational energy of the reactants.[5] Similar experiments where the product molecules were deflected in an electric field to separate them according to their average rotational velocities (the most rapidly rotating molecules were deflected less because their dipole moments were more nearly averaged out to zero over all orientations of the molecules) even allowed estimation of the relative amounts of product excitation energy in rotational and vibra-

tional modes.[11] The only reactive scattering experiments reported where internal states of molecules in the primary beams were selected are two measurements of the angular distributions of products scattered from collisions of K and Rb with orientation-selected CH_3I.[12,13]

It is anticipated that with the further advances in technology necessary to do more completely definitive experiments, molecular beam techniques will come to occupy the same status with regard to the study of chemical reactions that spectroscopy now occupies in the understanding of molecular structure.

C. Summary of Previous Work on the $N_2^+ + H_2$, HD, D_2 Reactions

The $N_2^+ + H_2$ reaction was one of the very first gas phase ion-molecule reactions to be positively identified,[2] and, along with other isotopic hydrogen atom transfer reactions with noble gas and organic ions, has been one of the most extensively studied. In early experiments designed to measure rate constants at near-thermal energies Gutbier,[14] and Schissler and Stevenson[15] studied, respectively, the reactions

$$N_2^+ + H_2 \rightarrow N_2H^+ + H$$

and

$$N_2^+ + D_2 \rightarrow N_2D^+ + D$$

in conventional mass spectrometers and reported results neglecting the possibility of the reactions

$$H_2^+ + N_2 \rightarrow N_2H^+ + H$$

and

$$D_2^+ + N_2 \rightarrow N_2D^+ + D$$

in the mixture leading to the same products.

The later experiments of Giese and Maier,[16] using a tandem mass spectrometer with extraction of secondary ions parallel to the primary beam, determined the energy dependence of the total reaction cross section for $N_2^+ + D_2$ from about 0.5 eV to 15 eV, and showed that the reaction with D_2^+ was not negligible in the previous work. Due to the inability of the apparatus to collect all the product ions emerging over the entire possible angular distribution, however, Giese and Maier found it necessary to include a correction of about +25% based on the form of the product angular distribution, which they assumed was isotropic in the center of mass (CM) coordinate system.

Turner, Fineman and Stebbings[17] extended the total cross section measurements for $N_2^+ + D_2$ to 70 eV, using a tandem mass spectrometer where the ion beam was crossed with a neutral beam. They also reported the first crossed beam measurements of the product angular distribution from an ion-molecule reaction, using $N_2^+ + D_2$. Due to poor resolution the angular distribution results yielded little information concerning the dynamics but clearly contradicted the assumption of isotropic scattering. The total cross section results agreed with those of Giese and Maier within about a factor of two in the region of overlap.

Previous work on the $N_2^+ + HD$ reactions has been limited to measurements made with a conventional mass spectrometer by Moran and Friedman.[18] The total cross sections for formation of $N_2H^+ + N_2D^+$ and the isotope ratio were determined at average ion energies up to about 6 eV. The theoretical analysis included reactions leading to these products from

either N_2^+ or HD^+.

The reactions of N_2^+, Ar^+ and CO^+ with isotopic hydrogen molecules are natural choices for first studies of ion-molecule reaction dynamics because of their large cross sections and the high ion to neutral mass ratio of both reactants and products, which by conservation of momentum confines the product ions to a small range of laboratory scattering angles.[19] The first experiments which directly yielded information on the dynamics of ion-molecule reactions were those of Lacmann and Henglein,[20] who measured the velocity spectra of ions scattered near zero degrees in the laboratory (LAB) coordinate system from reactions of Ar^+, N_2^+ and CO^+ with H_2 and D_2 as a function of primary ion energy in the range 25-200 eV. In their apparatus a non-selected primary ion beam was passed through a cell containing the target gas and the products emerging nearly parallel to the primary beam analyzed by means of a crossed magnetic and electric field velocity selector (without mass analysis). These authors found that the product ion distribution was strongly peaked forward of the CM velocity at all beam energies. They interpreted these results in terms of a "stripping model" (SM), in which the hydrogen atom not picked up by the ion receives no momentum from the collision, though the data showed considerable deviation from the predictions of this model at the higher energies.

With a much more sophisticated ion beam-collision cell apparatus employing mass and energy selection of both the primary beam and product ions, Doverspike, Champion and Bailey[21] measured the energy (and some angular) distributions for the Ar^+ and N_2^+ reactions with D_2 between 2 and 100 eV. Obtaining results in close agreement with those of

Lacmann and Henglein for the peak velocity of forward scattered products, these workers found in addition for some primary beam energies a small peak at velocities smaller than that of the CM, corresponding to 180° CM scattering. They drew the conclusions that the energetics are consistent with "activated complex" formation at low kinetic energies, a "pickup" mechanism at moderate energies, and a third process at the high energies which leads to less internal excitation in the product ion than predicted by the stripping model. No significant differences were found in the energetics of the N_2^+ and the Ar^+ reactions.

Finally, a study has very recently been reported by Herman, Kerstetter, Rose and Wolfgang,[22] who used a crossed beam apparatus (without primary ion mass selection) to determine the energy and angular distributions of products from the N_2^+ and $Ar^+ + D_2$ reactions at energies between 0.7 eV and 25 eV. Even at the lowest energies agreement was obtained between the experimental data and a "modified stripping model" in which the trajectories of reactants and products are influenced by an r^{-4} polarization attraction, though the atom transfer itself is subject to the stripping model conditions. The idea of a long-lived collision complex at any relative energy was rejected.

D. The Present Experiments

Results are reported here for the distributions in energy and angle for both N_2H^+ and N_2D^+ products from reactions of N_2^+ with H_2, HD and D_2. These experiments were undertaken in order to investigate the isotope effects on the dynamics and to determine unambiguously the features of the CM angular distributions of products which, particularly for the large CM angle scattering, were barely touched upon in the previous work.

The data cover the primary ion energy range from 25 eV, where the large angle scattering is barely resolved, up to 135 eV, and include data on the energy variation of the intensity at each part of the angular distribution, in addition to the energetic data. For three primary beam energies each in the H_2 and D_2 reactions, contour maps showing the complete product ion velocity and angular distributions in the CM coordinate system are presented in order to demonstrate clearly the isotope and relative kinetic energy effects on the features of the distributions. These are the only such complete distributions yet reported for a chemical reaction.

As expected, the correlation of energetic, intensity and isotope effect data provide the basis for a much more rigorous comparison with various models for the dynamics than is possible from the limited data reported previously for these reactions.

II. Instrumentation and Operating Procedure

A. General Description of the Apparatus

The apparatus and procedure used for these experiments have been described in detail in a previous report;[19] therefore only a brief description is included here.

The N_2^+ ions are created in a low-pressure source (10^{-3} torr) by bombardment with electrons of 50-70 eV energy. After extraction from the source with a potential of about -250 V, the ions are focused with a series of electrostatic lenses into a magnetic momentum analyzer, which gives both mass and velocity separation of the ions. The analyzed beam is then collimated with a second set of electrostatic lenses, passing finally, under field-free conditions, through the entrance aperture of the collision cell containing the target gas. The exit aperture of the collision cell and the product ion analysis and detection system are coupled and rotate in the horizontal plane to measure the angular distribution. Ions emerging at the preset angle enter first a 90° spherical electrostatic energy analyzer, then are focused at low energy into an RF quadrupole field mass filter from which they are extracted by a high potential and detected with an ion counting system.

B. Operating Conditions and Procedure

Regardless of the final desired ion beam energy, the magnetic momentum analysis of the N_2^+ ions was done at an energy of 25 eV and the final acceleration accomplished in the last focusing stage. This procedure gave a uniform full-width at half maximum (FWHM) energy distribution in the primary beam estimated to be less than 0.5 eV.

After preparation of the primary beam and measurement of its energy and angular distribution, the collision cell was filled with the target gas to a pressure of 8-10 $\times 10^{-4}$ torr, and data collected by setting the detector mass filter to the appropriate mass number and scanning either the energy distribution at fixed angle or the angular distribution at fixed energy - recording at each point the number of counts, the time interval used (usually 20-30 sec), the angle and energy analyzer settings and the collision cell pressure. The peak primary beam intensity was recorded at intervals of 20-30 minutes and the small drift taken into account by using a linear interpolation for the intensity corresponding to each point in the interval. Background signals due to reactions outside the collision cell (where the pressure was a factor of 1000 lower than the collision cell pressure) were measured in the same way by emptying the collision cell and leaking gas into the main vacuum chamber to give the same background pressure of target gas. In the HD experiments however, it was necessary to monitor the collision cell pressure with the main chamber ion gauge to avoid isotopic mixing on the hot filament. All the data were normalized to the same pressure scale, and all the measured signals were linear with respect to the target gas pressure.

For most primary beam energies only the product ion energy distribution at zero degrees and the angular distribution at a velocity near that of the CM were measured. The contour diagrams were generated from the intensities measured in an approximately 25x25 matrix of energy and angular coordinates covering the entire area of the distribution.

C. Factors Affecting the Accuracy of Measurements

Isotopic purity

Since the ion beam was mass-analyzed, the purity of the gas used was not particularly important. The magnetic momentum analysis eliminated virtually all of the mass 29 ions due to the natural abundance of N^{15}. The background due to the few remaining $(N^{14}N^{15})^+$ ions did not interfere seriously with measurement of the N_2H^+ distribution because the peak energies did not coincide.

The target gases used were of the following sources and isotopic purities:

H_2	LRL	Natural Abundance
HD	Stohler Isotope	99.3%
D_2	Liquid Carbonic	98%

Peaks in the distribution profiles due to H_2 in the HD experiments and HD in the D_2 experiments were detectable, but since they were small and resolved from the other peaks, they did not affect the results.

Calibration of the energy analyzer

The spherical electrostatic energy analyzer in the detection system was calibrated by comparison with retarding potential measurements of ion energy and by the slope of the dependence of the peak intensity energy analyzer voltage on the ion source potential. An absolute accuracy of about 1% is estimated, but since the analyzer is an intrinsically linear instrument, relative energy values should be much more accurate than this.

Detector energy and angular resolution

The FWHM resolution of the energy analyzer was 3%, and the geometric full-width angular resolution defined by the diameters and separation of

the collision cell exit aperture and the detection system entrance aperture was 2.5°. These are, of course, values in the LAB system. In CM coordinates the resolution will be much less and will vary with both angle and velocity.

Mass resolution

The resolution of the quadrupole mass filter was set at about 35 for all of the experiments reported here. Separation of masses 28, 29 and 30 was complete to within the sensitivity of our detector.

Transmission in the detection system

The transmission of the energy analyzer, determined by the two 80% transmission grids used to attenuate the field at each end of the analyzer, was 64%. The transmission of the focusing system and mass filter combination after the energy analyzer was found to be constant with respect to the ion energy within the accuracy of the measurements (about 10%) and equal to about 50%.

Detection efficiency

The efficiency of the ion counter was virtually unity for all ions[19] and since the product ion intensities were never much greater than 10,000 counts/sec, the coincidence losses were negligible.

III. Results

A. Data Analysis

The following notation is used throughout the discussion:

M_i = initial ion mass

$\underset{\sim}{v}_i$ = initial ion LAB velocity

$\underset{\sim}{g}_i$ = initial ion CM velocity

E_i = initial ion LAB energy

M_f = final ion mass

$\underset{\sim}{v}_f$ = final ion LAB velocity

$\underset{\sim}{g}_f$ = final ion CM velocity

E_f = final ion LAB energy

m_i = initial neutral mass

$\underset{\sim}{u}_i$ = initial neutral LAB velocity

$\underset{\sim}{w}_i$ = initial neutral CM velocity

m_f = final neutral mass

$\underset{\sim}{u}_f$ = final neutral LAB velocity

$\underset{\sim}{w}_f$ = final neutral CM velocity

E_s^o = initial relative kinetic energy (in the CM system)

E_s = final relative kinetic energy (in the CM system)

Q = energy defect of the reaction = $E_s - E_s^o$

H_i = internal energy of reactants (excitation energy)

H_f = internal energy of products (excitation energy)

W = heat of reaction (difference between ground state energies of reactants and products)

θ = LAB polar scattering angle

χ = CM polar scattering angle

ϕ = azimuthal scattering angle

The scattering of two reactant particles to give two product particles can be described in terms of a Newton velocity vector diagram, which depicts the collision simultaneously in LAB and CM coordinates. Though the kinematics of reactive collisions has been treated by several authors,[6] a brief review is pertinent for the discussion which follows.

Figure 1 shows a vector diagram for the collision at point $\underline{O}$ in the LAB system, between an ion with velocity $\underset{\sim}{v}_i$ and a neutral with velocity $\underset{\sim}{u}_i$, in a space free from externally applied fields. The center of mass of the two particles, defined at any instant to be on the line between them at a point determined by the mass ratio, thus moves through space on a straight line with a velocity $\underset{\sim}{v}_{CM}$. Since the conservation of linear momentum requires that the motion of the center of mass be unchanged in the collision, the point $\underset{\sim}{v}_{CM}$ is a fixed reference point in $\underset{\sim}{v}$ space (for this collision) and may be taken as the origin of a coordinate system with the center of mass at rest (the CM system). In this new system the initial velocities of the ion and neutral are $\underset{\sim}{g}_i$ and $\underset{\sim}{w}_i$, respectively. They are related by

$$M_i \underset{\sim}{g}_i = -m_i \underset{\sim}{w}_i \quad . \tag{1}$$

After the collision the ion is found to have new LAB and CM velocities $\underset{\sim}{v}_f$ and $\underset{\sim}{g}_f$, with orientation specified by (θ, ϕ_{LAB}) in the LAB system and (χ, ϕ_{CM}) in the CM system. The velocity of the neutral particle after the collision (not shown) is determined by

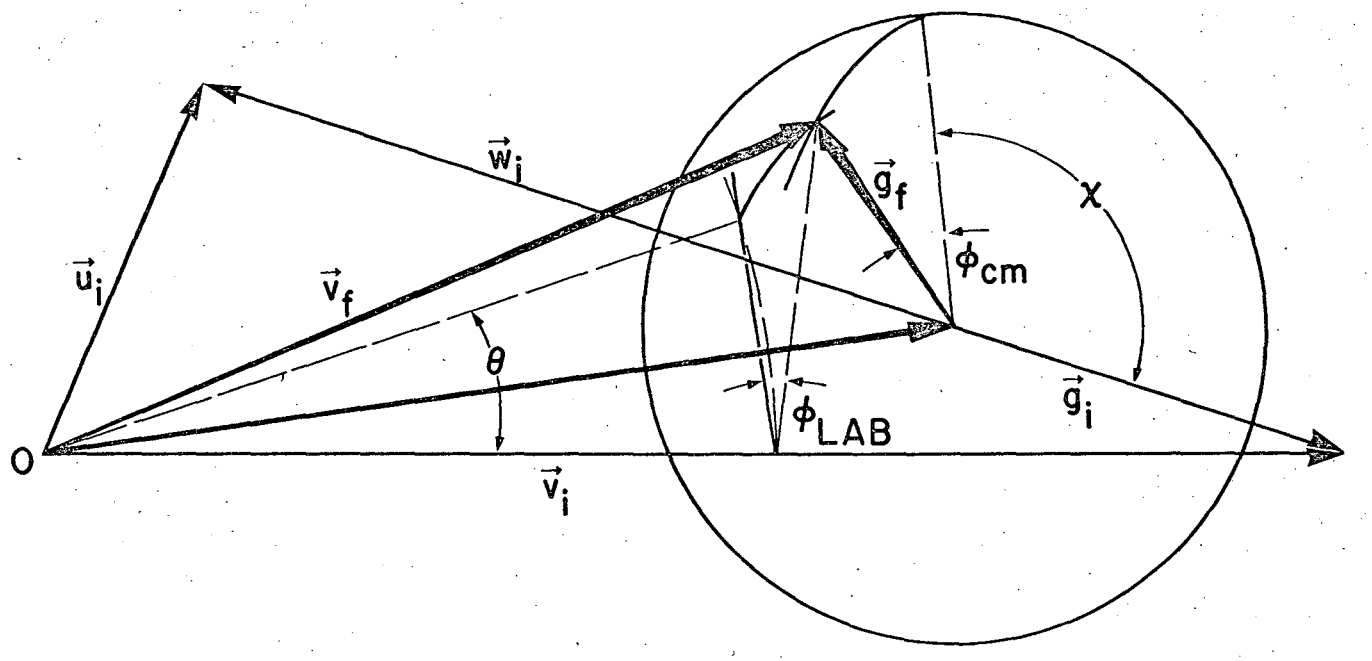

XBL 678-4784

Fig. 1 Newton velocity diagram for arbitrary initial ion and neutral velocities; showing relationships between initial and final LAB and CM coordinates.

$$M_f \underset{\sim}{g}_f = - m_f \underset{\sim}{w}_f \tag{2}$$

required, again, from conservation of momentum.

The total energy E_t available in the collision is

$$E_t = \frac{1}{2} m_i u_i^2 + \frac{1}{2} M_i v_i^2 + H_i + W \tag{3}$$

where H_i is the sum of whatever excitation energies (electronic, vibrational, rotational) the reactants may have and W is the heat of reaction. The total energy may be partitioned between that associated with motion of the center of mass (E_{CM}) and the energy available to the reactants in the CM system:

$$E_t = E_{CM} + E_s^o + H_i + W , \tag{4}$$

where

$$E_{CM} = \frac{1}{2}(M_i + m_i) \; v_{CM}^2 \tag{5}$$

and

$$E_s^o = \frac{1}{2} M_i g_i^2 + \frac{1}{2} m_i w_i^2 = \frac{1}{2}\left(\frac{M_i + m_i}{m_i}\right) M_i g_i^2 \tag{6}$$

E_t is, of course, conserved in the collision, and E_{CM} is conserved separately, since $\underset{\sim}{v}_{CM}$ is unchanged and the total mass is conserved ($M_i + m_i = M_f + m_f$). The total energy available in the CM coordinate system is therefore constant and we may write

$$E_s^o + H_i + W = E_s + H_f \tag{7}$$

where

$$E_s = \frac{1}{2}\left(\frac{M_f + m_f}{m_f}\right) M_f g_f^2 \tag{8}$$

and where H_f is the internal (excitation) energy in the products. The energetics of the collision can then be described by the amount of

energy Q converted between kinetic and internal energy in the process:

$$Q = E_s - E_s^o = H_i - H_f + W \tag{9}$$

The greatest possible net transfer of kinetic to internal energy is for $E_s = 0$, in which case $Q = - E_s^o$. All products having a given total excitation energy H_f must, under a defined set of initial conditions (E_s^o, H_i, W), have an ion velocity vector located on the surface of a sphere in $\underset{\sim}{v}$ space of radius g_f with its center at $\underset{\sim}{v}_{CM}$.

The energetics of the collision are then specified at every point in $\underset{\sim}{v}_f$ space. The distribution in intensity as a function of $\underset{\sim}{v}_f$ is however determined only by the details of the collision mechanism. The only a priori requirement on the intensity distribution from collisions of the type diagrammed in Fig. 1 is that in an experiment where the orientation of the particles is not selected the distribution must be cylindrically symmetric about the relative velocity vector ($\underset{\sim}{g}_i - \underset{\sim}{w}_i$), since any orientation ϕ_{CM} of the initial plane of the collision in the CM system (which is in general different from the plane of $\underset{\sim}{v}_i$ and $\underset{\sim}{u}_i$) is equally probable.

In a collision cell experiment one has, of course, not a single value of $\underset{\sim}{u}_i$, but a Maxwellian distribution of neutral velocities isotropically distributed around the scattering center. The particles in the ion beam will also have some finite distribution in velocity and angle. The resultant distribution in $\underset{\sim}{v}_{CM}$ will then be the convolution of the initial neutral and ion velocity vector distributions, each reduced by the appropriate mass factor $\frac{m_i}{M_i + m_i}$ and $\frac{M_i}{M_i + m_i}$, respectively.

For the experiments reported here the most probable value of the neutral speed u_i is in general less than 10% of v_i. If the cross section

for the process being studied varies slowly over the range of initial relative velocities, then the energetics for the most probable value of the velocity $\underset{\sim}{g}_f$ at any scattering angle χ can be calculated using the most probable $\underset{\sim}{v}_i$, which can be measured, and the most probable $\underset{\sim}{u}_i$, which is $\underset{\sim}{u}_i = 0$. The velocity vector diagram for scattering under these conditions is shown in Fig. 2, where the initial velocities are to be interpreted as the most probable values.

Having $\underset{\sim}{u}_i = 0$ greatly simplifies the calculation of the energetics. First note that $\underset{\sim}{v}_{CM}$ is colinear with $\underset{\sim}{v}_i$, making the azimuthal angle ϕ the same in both the LAB and CM systems. The initial conditions are specified completely from the measurement of v_i or E_i:

$$w_i = v_{CM} = \frac{M_i}{M_i + m_i} v_i \tag{10}$$

$$g_i = \frac{m_i}{M_i + m_i} v_i \tag{11}$$

$$E_s^o = \frac{m_i}{M_i + m_i} E_i \quad . \tag{12}$$

The final relative speed g_f and relative kinetic energy E_s are determined by a measurement of v_f and θ only:

$$g_f^2 = v_f^2 - \frac{2M_i}{M_i + m_i} v_f v_i \cos\theta + \left(\frac{M_i}{M_i + m_i}\right)^2 v_i^2 \tag{13}$$

hence ϕ need not be measured. In fact, because the average relative velocity vector is colinear with $\underset{\sim}{v}_i$, by the above symmetry argument the intensity at a given v_f and θ (or g_f and χ) must be the same for all ϕ.

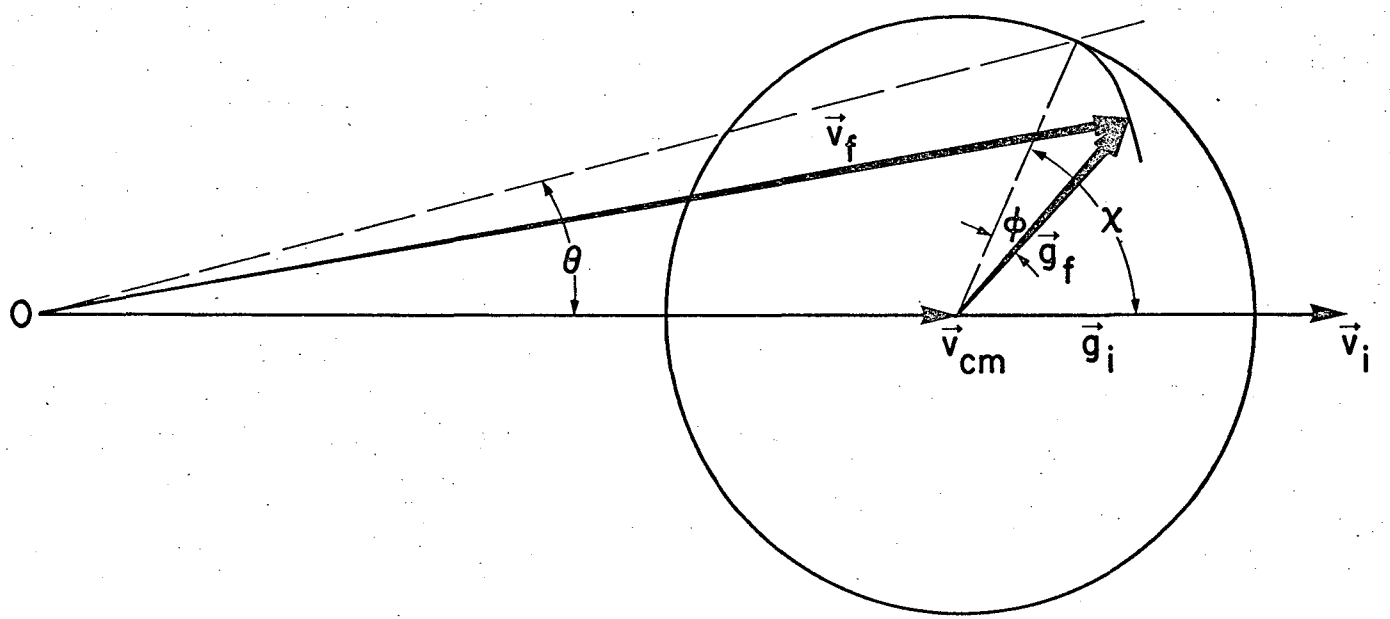

XBL 678-4785

Fig. 2 Newton velocity vector diagram for initial neutral velocity $\vec{u}_i = 0$, showing relationships between initial and final LAB and CM coordinates.

The quantity measured for each primary ion energy E_i in the experiments is the intensity (particles per unit time) striking the detector as a function of energy E_f and angle θ. The form in which the data is finally rendered is the relative differential cross section (averaged over the detector dimensions) for scattering of product ions into an element of volume

$$d^3\underset{\sim}{v} = v_f^2 \sin\theta \, d\theta \, d\phi \, dv_f = g_f^2 \sin\chi \, d\chi \, d\phi \, dg_f \qquad (14)$$

in the $\underset{\sim}{v}$ space diagrammed in Fig. 2. The equation used is

$$\bar{I}(\theta, v_f) = \bar{I}(\chi, g_f) = \frac{10^7 S \, f(\theta)}{t \, i^o P \, V_{EA}^{3/2}} \qquad (15)$$

where

S = number of counts recorded in time t (sec.)

P = collision cell pressure on a scale of 0 to 1000, where $1000 \cong 12 \times 10^{-4}$ torr

i^o = peak primary ion beam current through the energy analyzer in units of 10^{-12} amp

V_{EA} = energy analyzer potential (volts)

and where $f(\theta)$ is a factor which corrects for the different scattering volume subtended by the detector at different LAB angles, given by

$$f(\theta) = \frac{\text{scattering volume subtended by detector at } \theta = 0^\circ}{\text{scattering volume subtended by detector at angle } \theta.} \qquad (16)$$

This factor is calculated graphically assuming pressure cutoff at the collision cell apertures and varies from unity at $\theta = 0^\circ$ to 2.00 at $\theta = 8.5^\circ$, approximately the largest LAB angle at which products were found. The $V_{EA}^{3/2}$ factor normalizes the intensity to the change in

detection volume subtended (in $\underset{\sim}{v}$ space) as a function of E_f due to both the apparatus geometry and the transmission band of the energy analyzer, which is proportional to the energy transmitted. As demonstrated in the previous report[19] $\bar{I}$ is proportional to the true differential cross section in the limit as the resolution in initial conditions and detector volume is made infinitely good.

The calculations are done on the CDC 6600 computer at the LRL computer center. For each data point entered the computer prints out $\bar{I}$, E_f, v_f, θ, g_f, X, E_s and Q. In addition a CALCOMP plot is obtained of $\bar{I}$ vs. v_f for each constant angle profile and of $\bar{I}$ vs. θ for each constant energy profile measured.

B. Contour Maps of the Complete Product Ion Distributions

To generate each contour line all the coordinate pairs (v_f,θ) corresponding to a selected $\bar{I}$ measured from the constant angle and constant energy profiles for that experiment were fed into the computer, which transformed each pair of coordinates and plotted the points in the CM system (g_f,X). Smooth lines were drawn by hand through the points for each intensity and were superimposed to produce the maps.

The complete distributions in $\bar{I}(g_f,X)$ for the $N_2^+ + H_2$ reaction at primary ion energies of 47.00 eV, 84.32 eV and 121.68 eV are presented in Figs. 3, 4, and 6, and the distributions for the $N_2^+ + D_2$ reaction at primary ion energies of 24.93 eV, 65.00 eV and 89.84 eV are shown in Figs. 8, 9 and 11. Following the higher energy distributions, where the large angle scattering is clearly resolved, plots of the radial (constant X) peak value of $\bar{I}$ vs. X are given. The points denoted on the contour maps by small circles represent the positions of the peaks for large angle scattering measured from the individual profiles.

Several qualitative features of the distributions are immediately apparent. First is the symmetry of the distributions about the 0°-180° line, which provides a rigid check on the precision of the measurements. The slight asymmetries noted, such as the uniformly greater width of the distribution on the positive angle side, are necessarily due to asymmetries in the apparatus but seem not to affect the locations of the peaks. Some small asymmetries are unavoidable--such as in the ion beam momentum analyzer, where ions with slightly different momenta pass through the exit slit at different places. Next, the distributions appear to have the shape of craters with relatively uniform height around most of the rim, but with an extremely high "mountain" on the forward side peaked at 0°. At a relative kinetic energy of 3.1 eV the structure of the large angle scattering is barely resolved (peaks are distinguishable in the H_2 experiment, Fig. 3, and not in the D_2 experiment, Fig. 8, because of better ion beam resolution) but at higher energies the crater shape is clearly defined. The "walls" of the crater grow steeper and more separated with increasing ion energy and always show a smaller slope toward the center of the crater than on the outside of the rim. The 0° peak has an elliptical horizontal cross section which reflects the shape of the primary beam (due to the better resolution of the apparatus in velocity than in angle) rather than the actual small angle scattering. In fact, the dimensions of this peak show almost no spreading over those of the primary beam in any of the experiments. Some of the distributions also show peaking of intensity in the backward direction. Finally, it is noted that the values of g_f at the radial peaks in a given distribution are virtually constant for the large angle scattering (except for Fig. 3, which is poorly resolved), implying energetics independent of the scattering angle for X between 45° and 180°,

and that the large angle relative velocity for a given experiment is in general greater than the relative velocity for 0° scattering. Also, the scattering at all angles from D_2 gives products with greater CM velocities than occur for the H_2 reactions at the same relative kinetic energy, because at identical ion-neutral separation the center of mass point is almost twice as far from the N_2D^+ product than the N_2H^+ product.

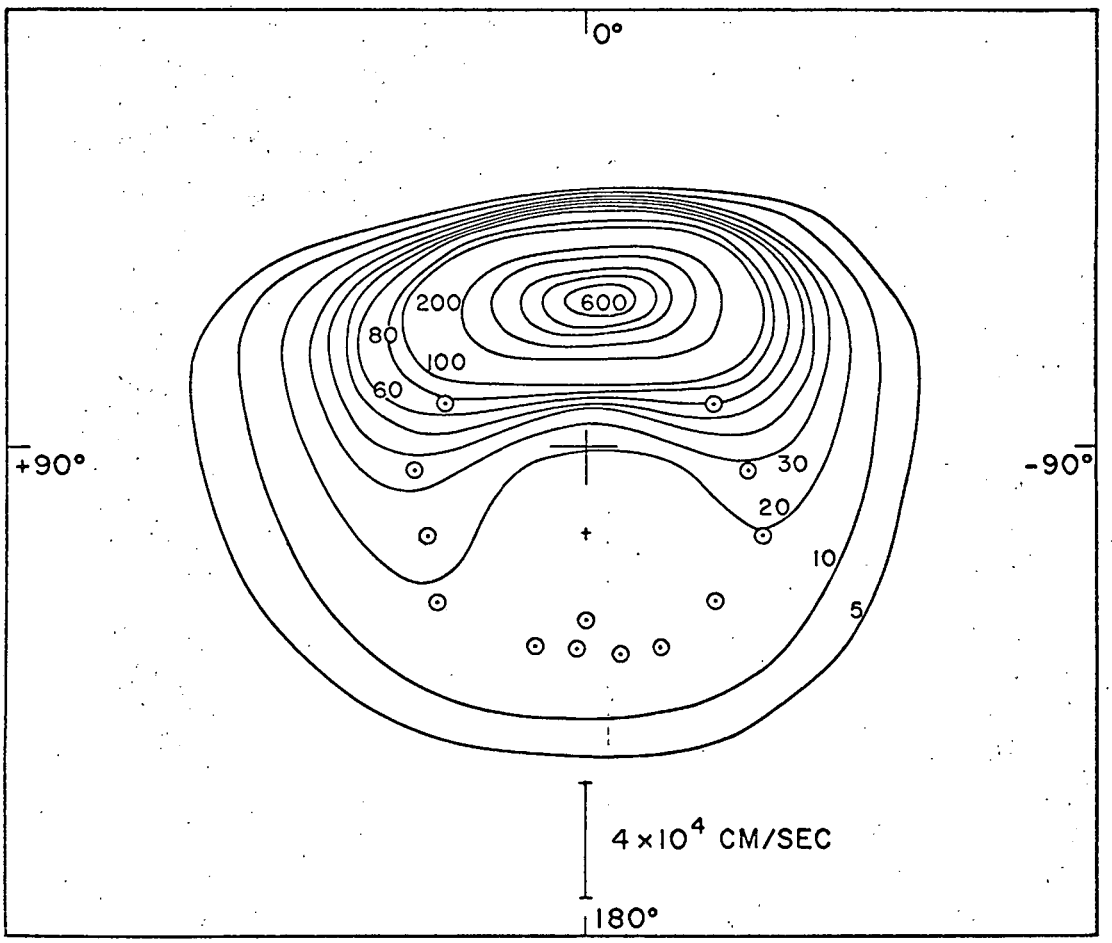

XBL 678-4782

Fig. 3 Contour map of N_2H^+ distribution in the CM coordinate system (g_f, χ) from the reaction

$$47.00 \text{ eV } N_2^+ + H_2 \rightarrow N_2H^+ + H \qquad \text{Exp't (199)}$$

The values of $\bar{I}$ (in units of 10^3) for the contour lines not labelled can be obtained by linear interpolation or extrapolation. The small circles indicate the locations of maxima in the constant energy and constant angle profiles.

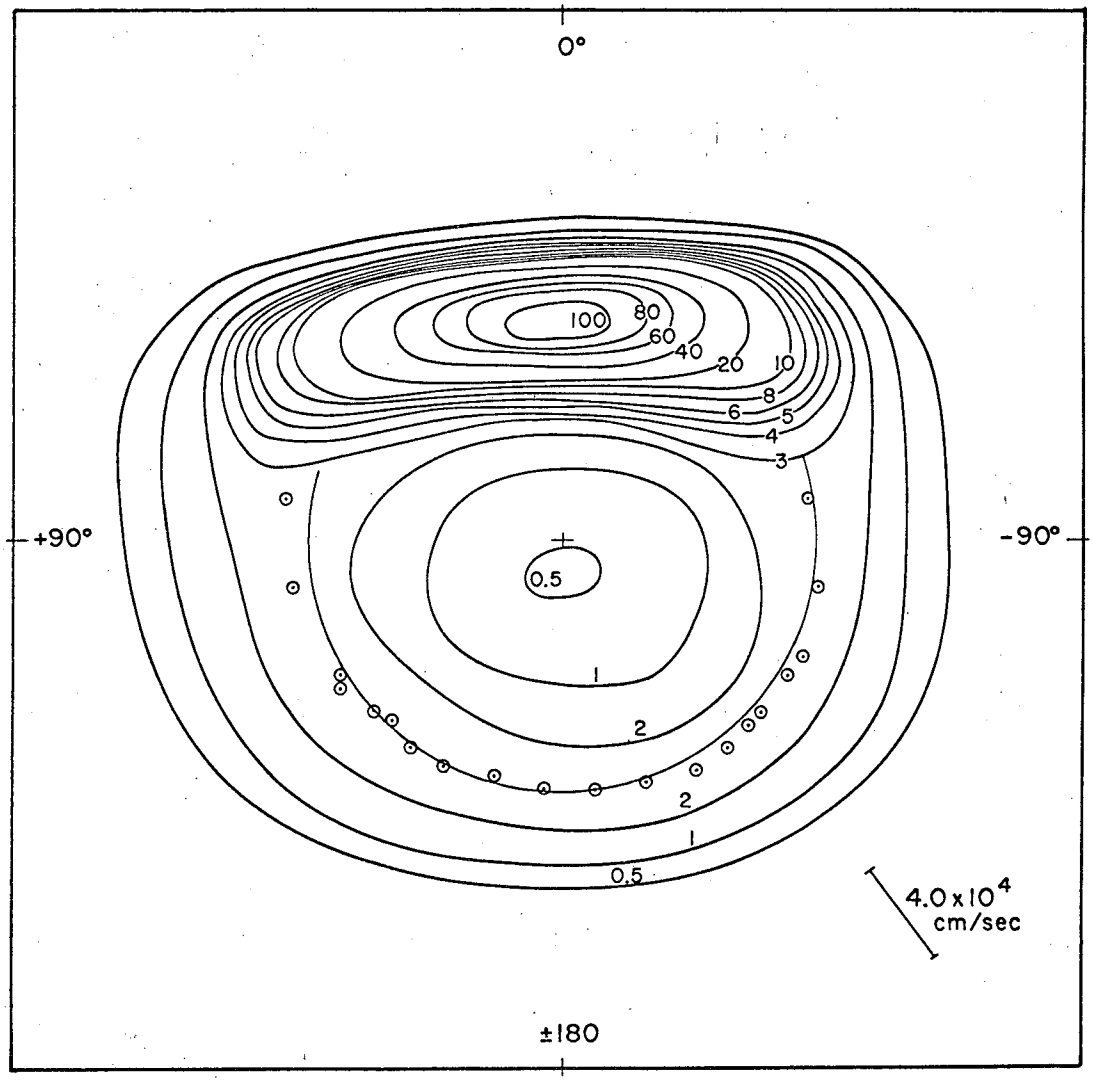

XBL 678-4796

Fig. 4 Contour map of N_2H^+ distribution in the CM coordinate system (g_f, X) from the reaction

$$84.32 \text{ eV } N_2^+ + H_2 \rightarrow N_2H^+ + H \qquad \text{Exp't (195)}$$

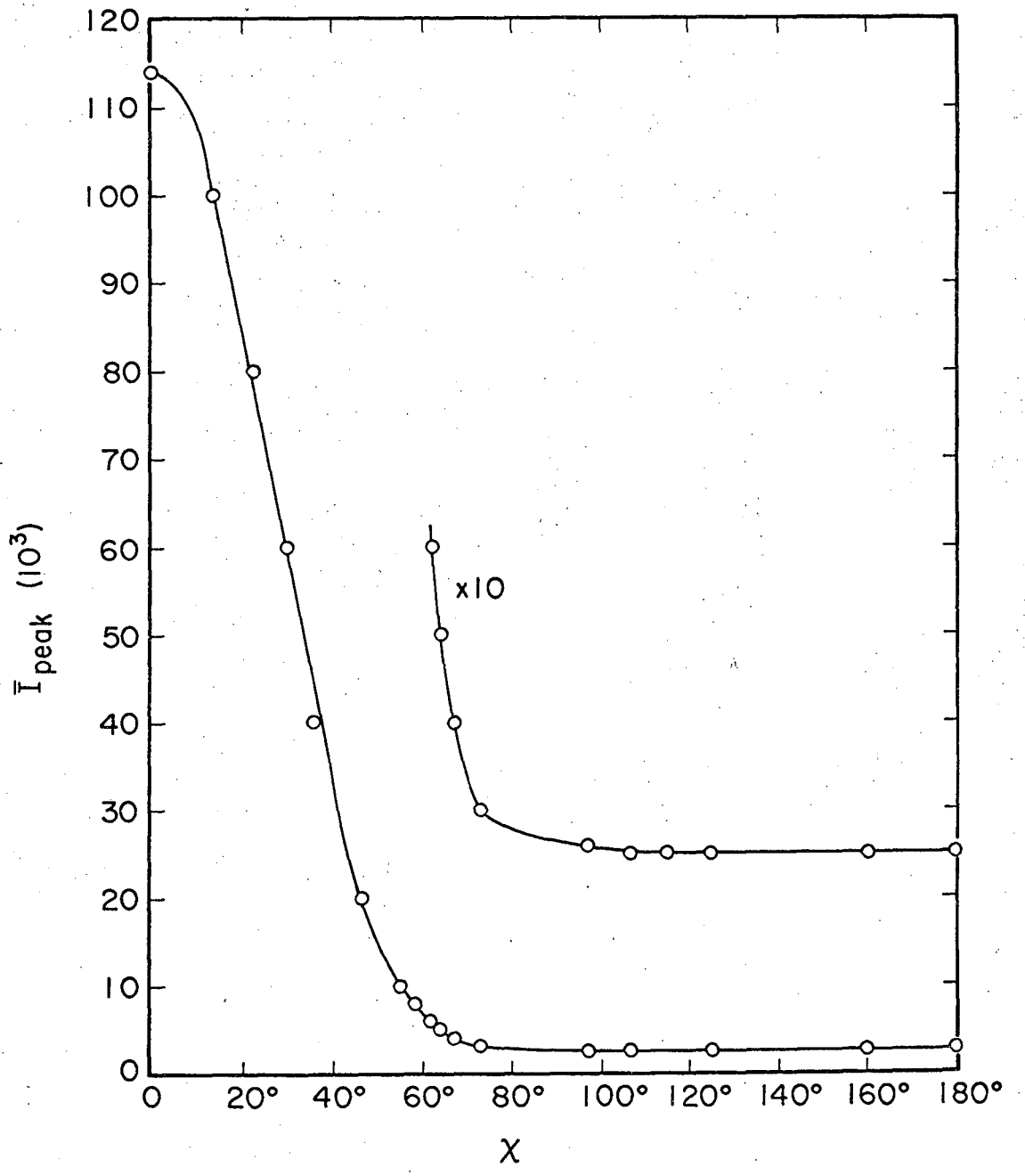

XBL 678-4789

Fig. 5 Radial peak intensity vs. CM angle

84.32 eV $N_2^+ + H_2 \rightarrow N_2H^+ + H$ Exp't (195)

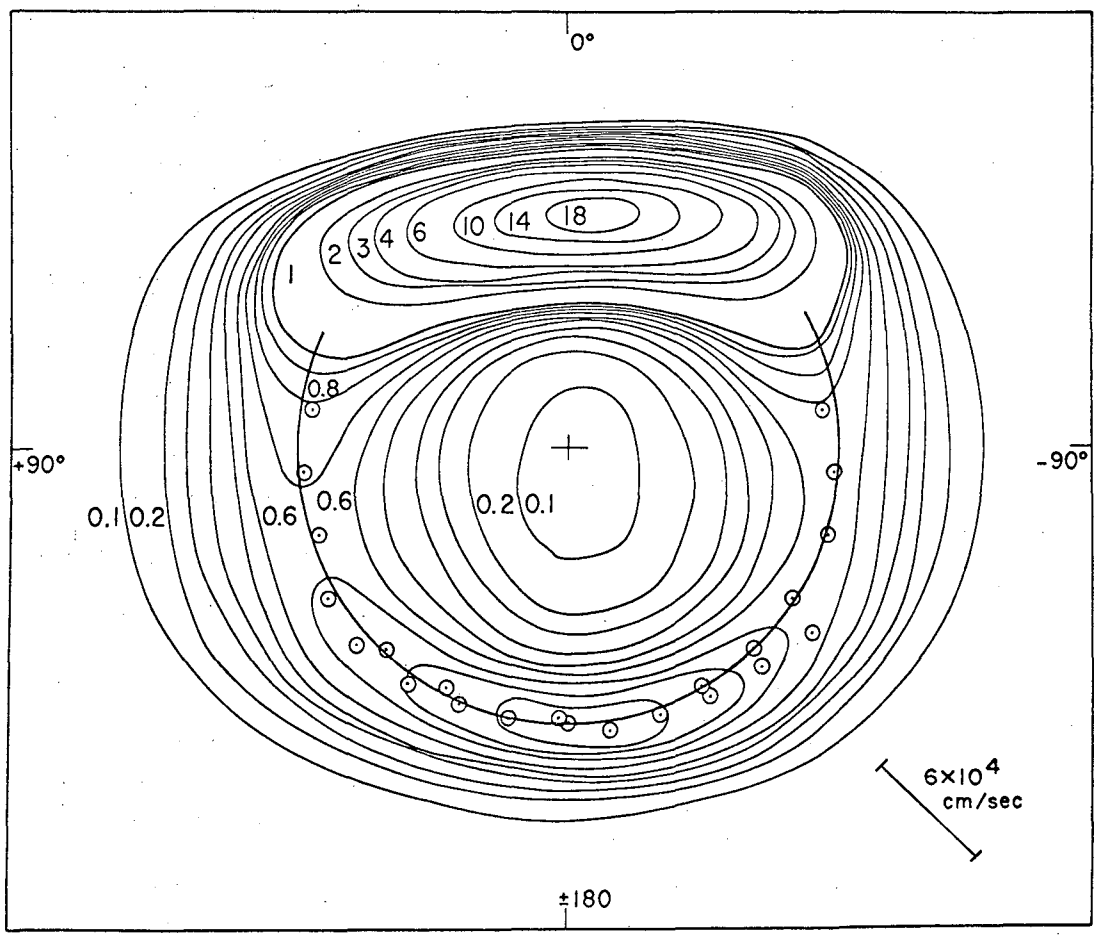

XBL 678-4800

Fig. 6 Contour map of N_2H^+ distribution in the CM coordinate system (g_f, χ) from the reaction

$$121.68 \text{ eV } N_2^+ + H_2 \rightarrow N_2H^+ + H \qquad \text{Exp't (200)}$$

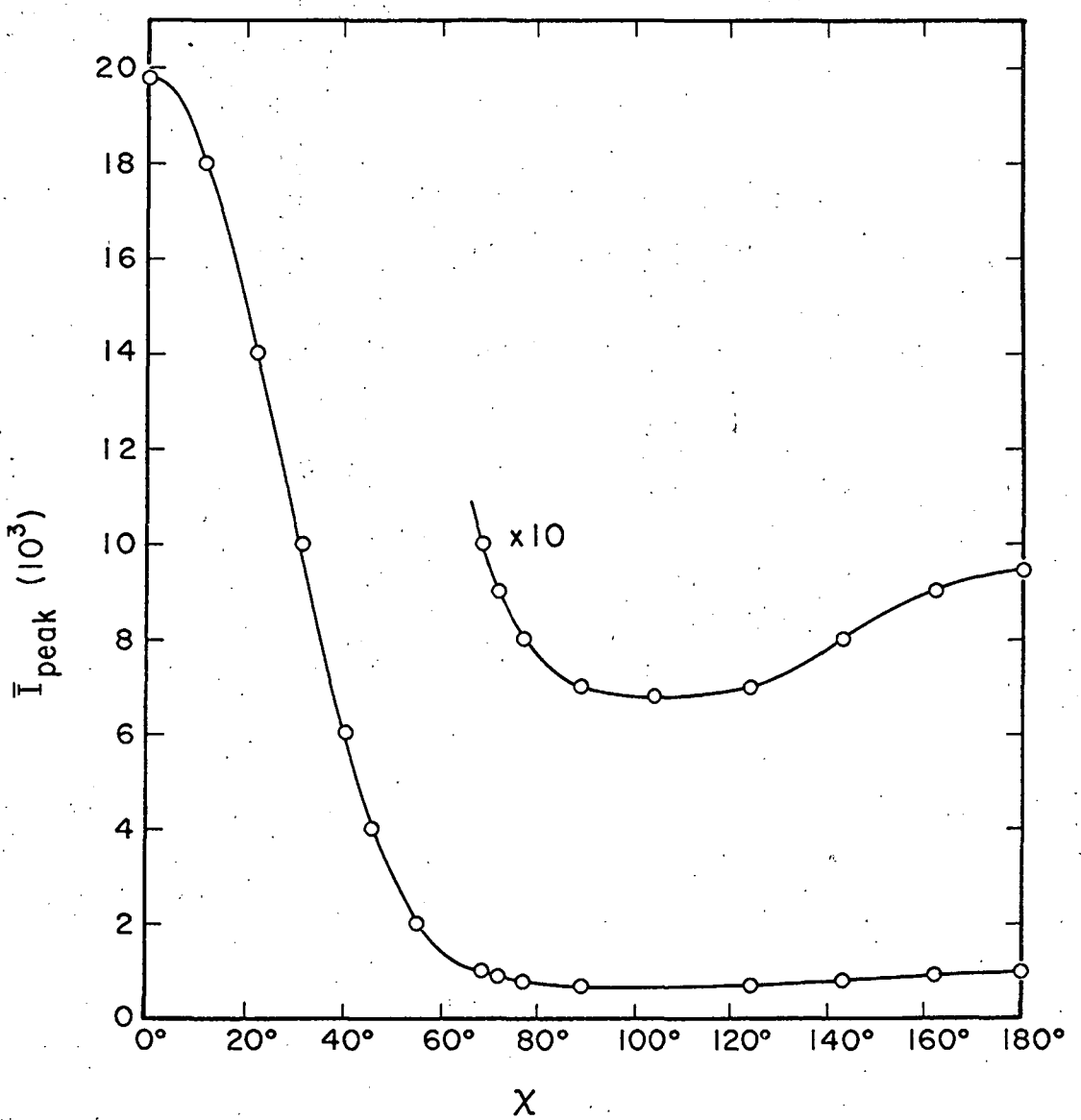

XBL 678-4791

Fig. 7 Radial peak intensity vs. CM angle

121.68 eV $N_2^+ + H_2 \rightarrow N_2H^+ + H$ Exp't (200)

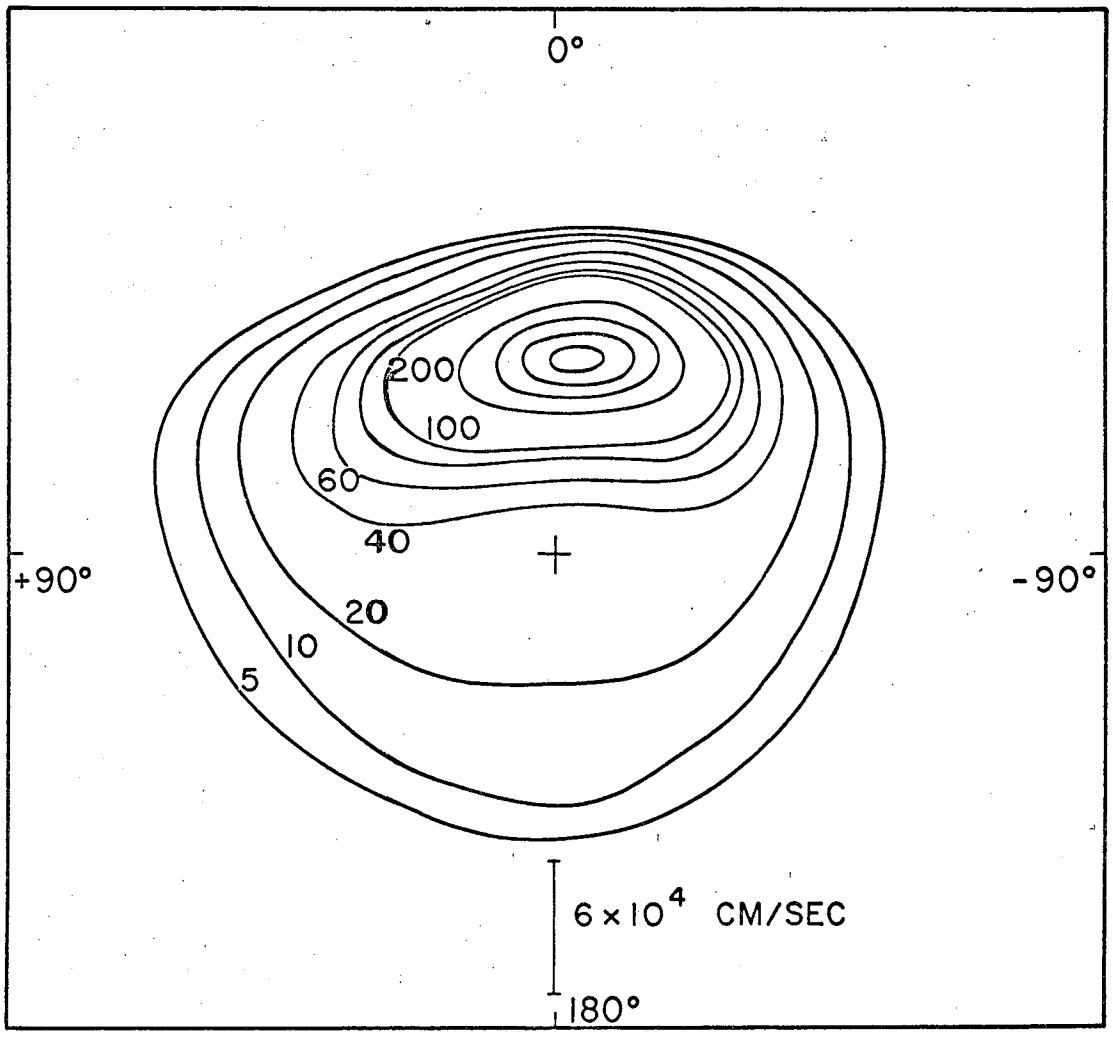

XBL 678-4780

Fig. 8 Contour map of N_2D^+ distribution in the CM coordinate system (g_f, χ) from the reaction

$$24.93 \text{ eV } N_2^+ + D_2 \rightarrow N_2D^+ + D \qquad \text{Exp't (190)}$$

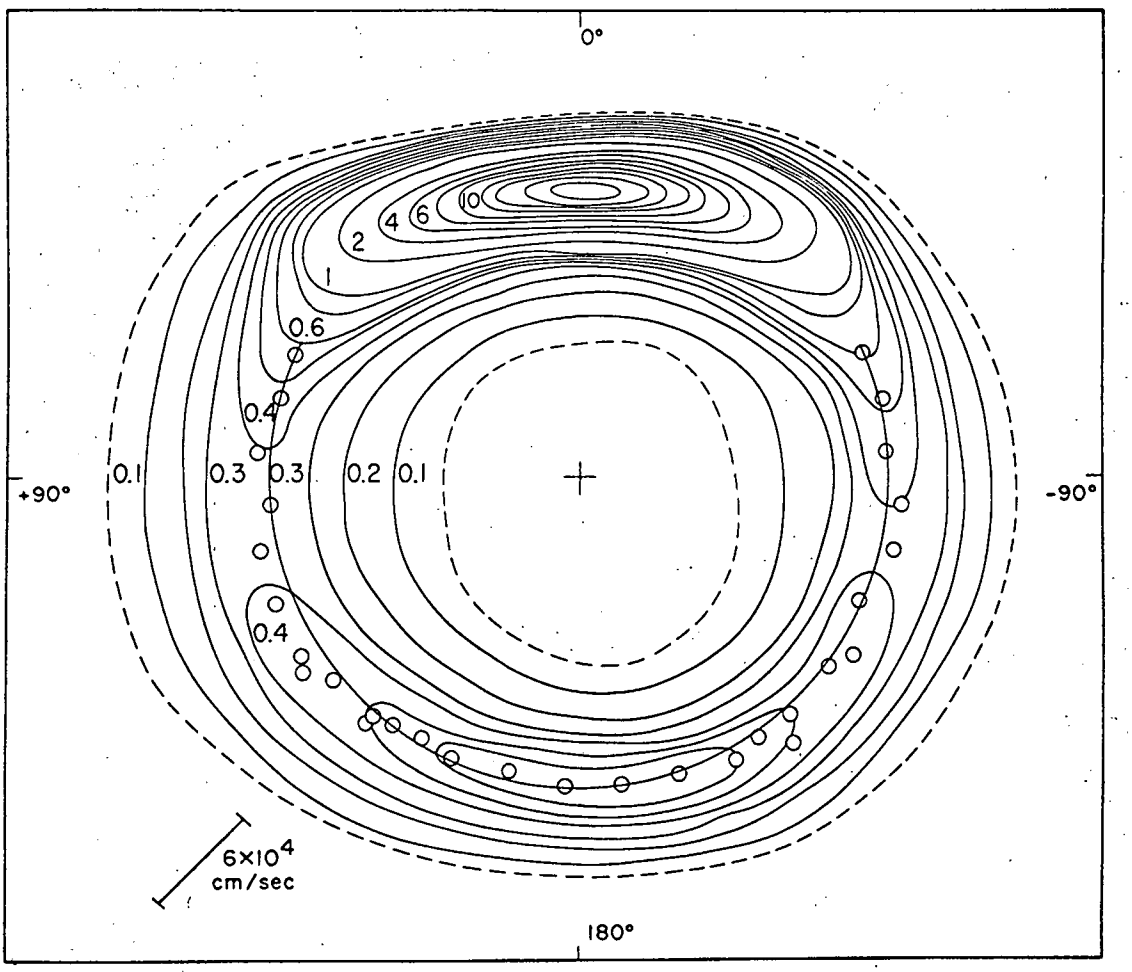

XBL 678-4799

Fig. 9 Contour map of N_2D^+ distribution in the CM coordinate system (g_f, χ) from the reaction

$$65.00 \text{ eV } N_2^+ + D_2 \rightarrow N_2D^+ + D \qquad \text{Exp't (186)}$$

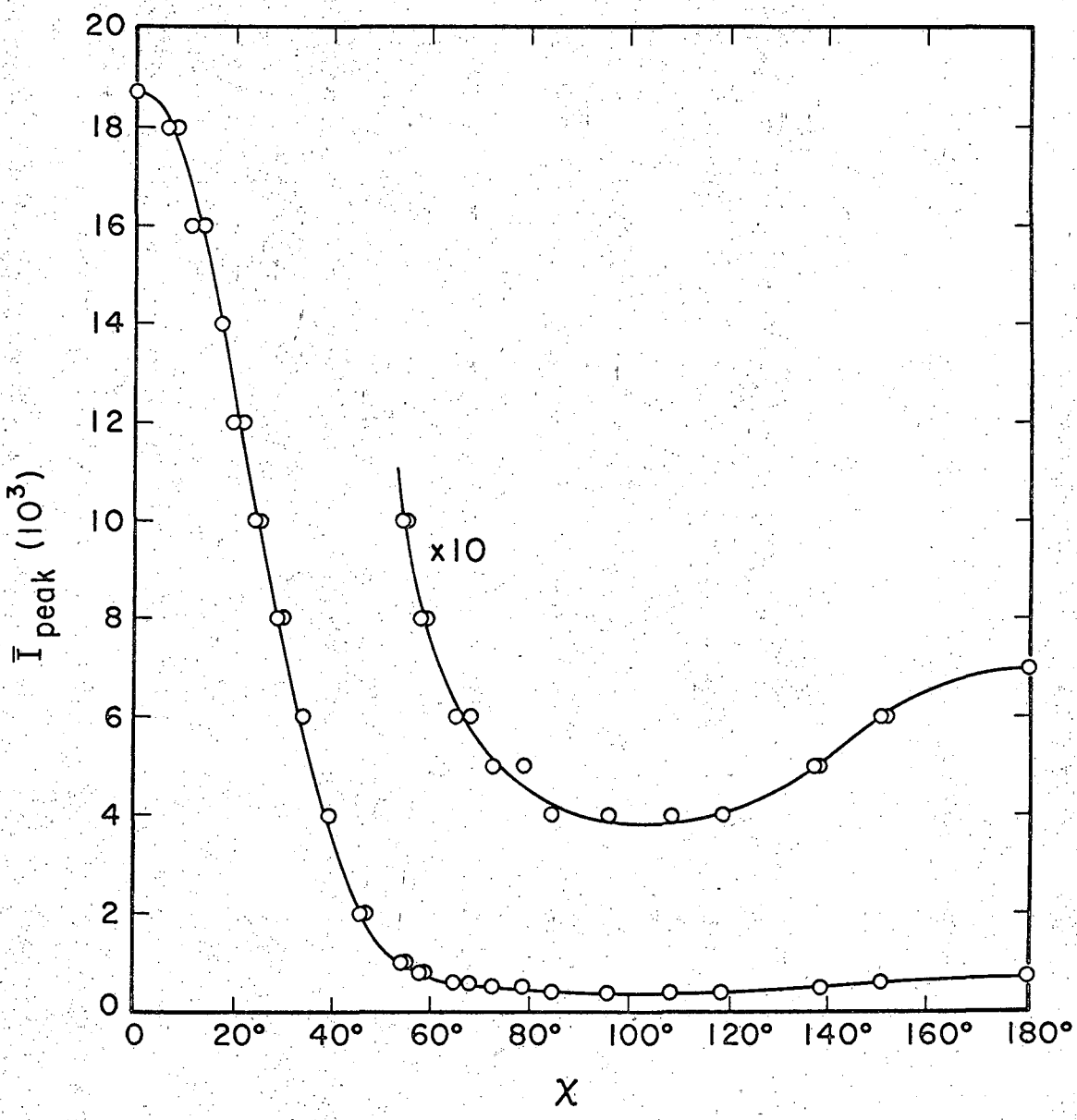

XBL 678-4790

Fig. 10 Radial peak intensity vs. CM angle.

65.00 eV $N_2^+ + D_2 \rightarrow N_2D^+ + D$ Exp't (186)

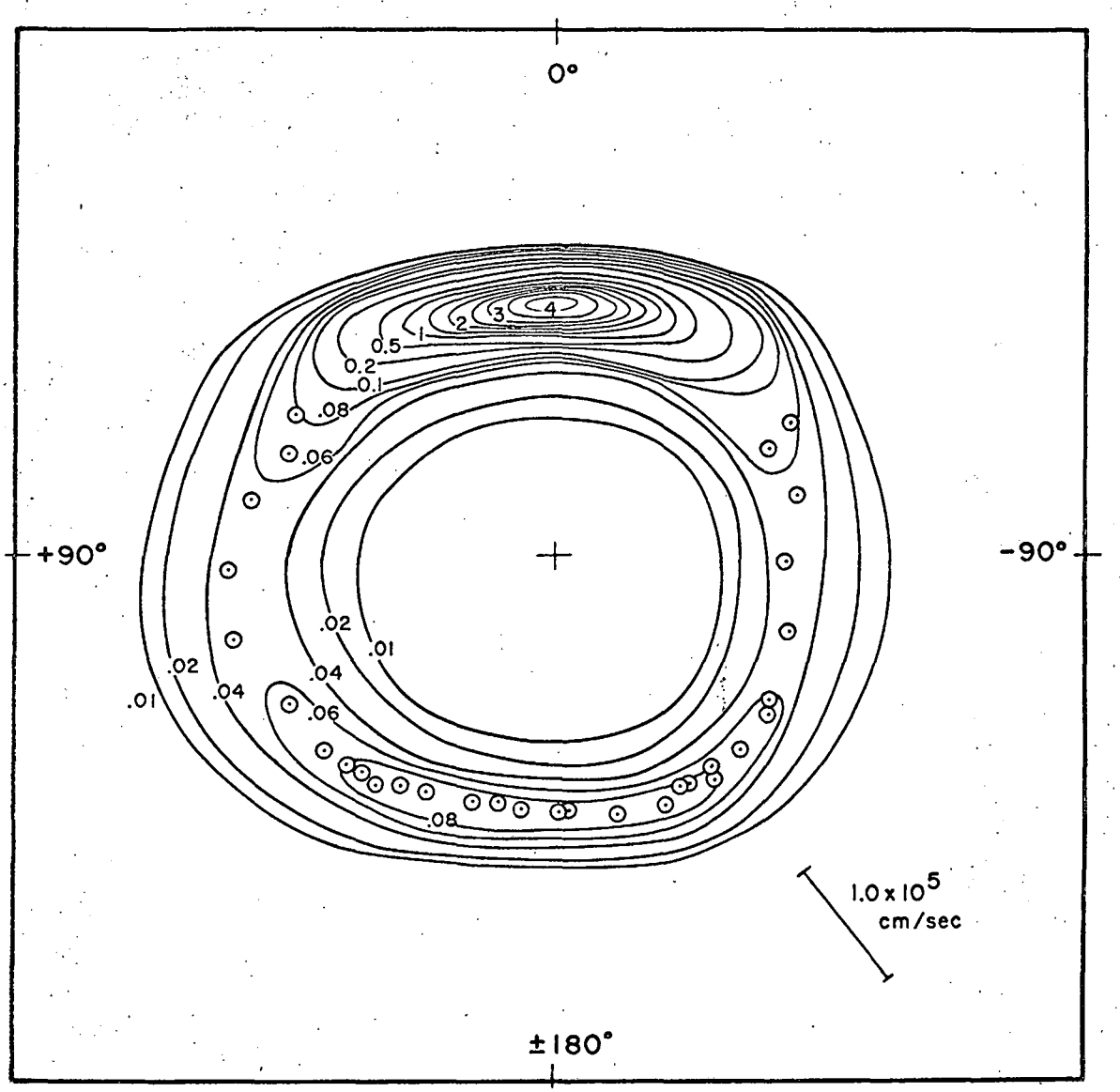

XBL 678-4781

Fig. 11 Contour map of N_2D^+ distribution in the CM coordinate system (g_f, X) from the reaction

$$89.84 \text{ eV } N_2D^+ + D_2 \rightarrow N_2D^+ + D \qquad \text{Exp't (193)}$$

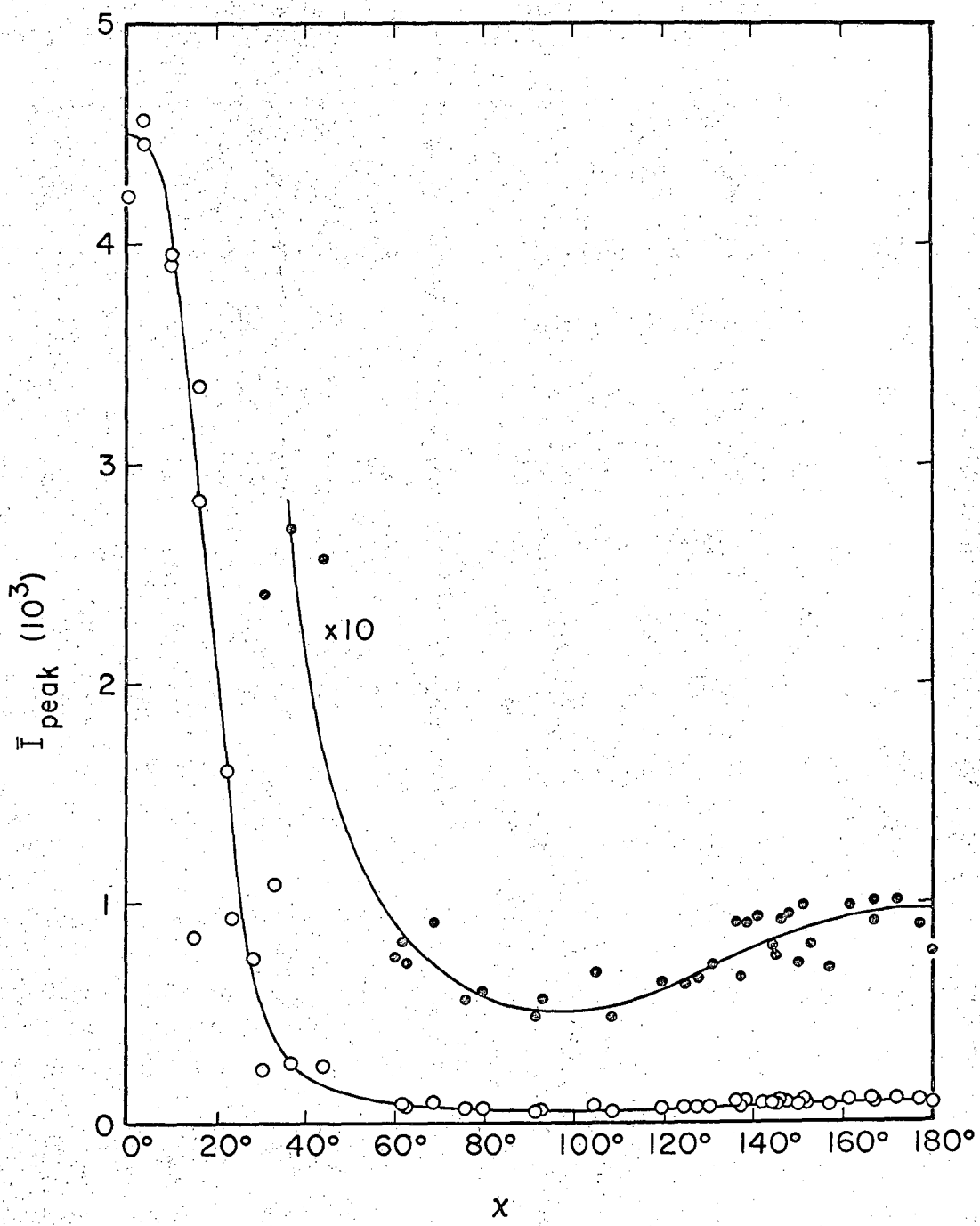

XBL 678-4795

Fig. 12 Radial peak intensity vs. CM angle

89.84 eV $N_2D^+ + D_2 \rightarrow N_2D^+ + D$ Exp't (193)

C. Energetic and Intensity Data

Tables I and II contain a summary of all the experimental data on the energetics and intensities for 0° and large angle scattering measured at the peaks in the radial profiles of the distributions. The quantitative features of the energetics may be best discussed with reference to various models for the collisions, which are treated in the next section. A quick glance at Table I shows, however, that the Q values do not change drastically with the isotope or the primary ion energy and are all negative, implying a net transfer of kinetic to internal energy in every reaction. Also, the endothermicity is usually greater for 0° scattering than for scattering through large angles.

The intensity data show both large variations with energy and large isotope effects. In Fig. 13 $\log \bar{I}_{0°}$ is plotted against E_i for all the reactions studied. It is seen that $\bar{I}_{0°}$ falls quite rapidly with increasing energy and is on the average about a factor of ten higher for the N_2H^+ product than for N_2D^+. Figure 14 shows the variation of $\bar{I}_{180°}$ with energy. In this plot because the distribution is slowly varying with respect to angle (as opposed to the 0° peak, where the angular width is little greater than that of the primary beam) the peaks in the differential cross sections are normalized to the same solid angle element by multiplication by g_f^2. The amounts of large angle scattering vary much more slowly with energy than do the 0° peaks, and show a nearly exponential dependence. The isotope effects are radically different than for small angle scattering. They show, for example, the N_2D^+ product from HD favored over the N_2H^+ product at 180°. This difference shows up most clearly in Fig. 15, in which the ratio of backward to forward scattering

in the CM coordinate system is plotted as a function of the initial relative kinetic energy. Finally, the relative amounts of backward peaking in the large angle scattering can be seen from the plot of $\bar{I}_{90°}/\bar{I}_{180°}$ given in Fig. 16. At low energies $\bar{I}_{90°}$ is greater than $\bar{I}_{180°}$ for all the reactions, but at high energies peaking at 180° is observed in all cases except the N_2H^+ product from HD. This feature is especially prominent in the case of the N_2D^+ product from HD, where $\bar{I}_{180°}$ goes to values greater than a factor of 5 higher than $\bar{I}_{90°}$.

Table I. Energetics

Exp't. No.	E_i (eV)	E_s^o (eV)	v_i (10^5 cm/sec)	0° Scattering v_f (10^5 cm/sec)	0° Scattering g_f (10^5 cm/sec)	0° Scattering E_s (eV)	0° Scattering Q (eV)	Large Angle Scattering v_f (10^5 cm/sec)	Large Angle Scattering g_f (10^5 cm/sec)	Large Angle Scattering E_s (eV)	Large Angle Scattering Q (eV)
$N_2^+ + D_2 \rightarrow N_2D^+$											
*186	65.000	8.1250	21.1784	20.037	1.506	5.635	-2.49	16.899	1.632	6.615	-1.51
187	24.955	3.1193	13.1223	12.298	0.816	1.654	-1.47	10.693	0.789	1.547	-1.57
188	35.068	4.3835	15.5558	14.560	0.949	2.237	-2.15	12.539	1.072	2.855	-1.53
189	75.000	9.3750	22.7492	21.530	1.624	6.552	-2.82	18.126	1.780	7.871	-1.50
*190	24.932	3.1165	13.1163	12.327	0.850	1.795	-1.32	---	---	---	--
191	44.955	5.619	17.6126	16.500	1.089	2.946	-2.67	14.223	1.188	3.506	-2.11
192	54.864	6.858	19.4571	18.337	1.312	4.276	-2.58	15.670	1.355	4.561	-2.30
*193	89.841	11.230	24.8985	23.615	1.829	8.311	-2.92	19.890	1.896	8.931	-2.30
$N_2^+ + H_2 \rightarrow N_2H^+$											
194	34.886	2.326	15.5154	15.000	0.519	1.213	-1.11	---	---	---	--
*195	84.318	5.621	24.1211	23.330	0.817	3.006	-2.62	21.582	0.931	3.903	-1.72
196	70.091	4.673	21.9921	21.210	0.684	2.107	-2.57	19.738	0.788	2.796	-1.88
197	110.227	7.349	27.5791	26.690	0.949	4.055	-3.29	24.576	1.165	6.111	-1.24
198	133.864	8.924	30.393	29.481	1.115	5.597	-3.33	27.063	1.303	7.645	-1.28
*199	47.000	3.133	18.0088	17.330	0.522	1.227	-1.89	16.221	0.587	1.552	-1.56
*200	121.682	8.112	28.9767	28.075	1.030	4.777	-3.34	25.817	1.228	6.790	-1.32
$N_2^+ + HD \rightarrow N_2D^+$											
207a.	44.841	4.339	17.5903	16.480	0.592	1.687	-2.65	15.108	0.780	2.928	-1.41
208a.	59.841	5.791	20.3205	19.143	0.789	2.996	-2.80	17.424	0.930	4.163	-1.63
210a.	74.909	7.249	22.7354	21.478	0.943	4.280	-2.97	19.475	1.060	5.408	-1.84
211a.	89.864	8.697	24.9016	23.618	1.126	6.103	-2.59	21.397	1.095	5.771	-2.73
212a.	105.364	10.197	26.9638	25.608	1.254	7.569	-2.63	23.146	1.208	7.024	-3.17
213a.	119.455	11.560	28.7103	27.322	1.390	9.300	-2.26	24.608	1.324	8.438	-3.12
214a.	35.046	3.392	15.5508	14.492	0.436	0.915	-2.48	---	---	---	--
$N_2^+ + HD \rightarrow N_2H^+$											
207b.	44.841	4.339	17.5903	16.962	1.074	2.681	-1.66	14.750	1.138	3.013	-1.33
208b.	59.841	5.791	20.3205	19.605	1.251	3.641	-2.15	17.000	1.354	4.265	-1.53
210b.	74.909	7.249	22.7354	21.947	1.412	4.638	-2.61	18.940	1.595	5.919	-1.33
211b.	89.864	8.697	24.9016	24.120	1.628	6.166	-2.53	20.765	1.727	6.939	-1.76
212b.	105.364	10.197	26.9638	26.188	1.834	7.825	-2.37	22.480	1.874	8.170	-2.03
213b.	119.455	11.560	28.7103	27.925	1.993	9.241	-2.32	23.935	1.997	9.278	-2.28
214b.	35.046	3.392	15.5508	14.967	0.911	1.931	-1.46	13.187	(0.859)	(1.717)	(-1.68)

* Contour map of product distribution determined

Table II. Intensities

Exp't No.	E_i(eV)	E_s° (eV)	$\bar{I}_{0°}$	$\bar{I}_{180°}$	$\bar{I}_{90° \pm 10°}$
$N_2^+ + D_2 \rightarrow N_2D^+ + D$					
*186	65.00	8.125	18.7×10^3	700	380
187	24.96	3.119	305	2700	6400
188	35.07	4.384	297	2000	4150
189	75.00	9.375	9.8	370	213
*190	24.93	3.117	515	-	-
191	44.96	5.619	212	4700	3070
192	54.86	6.858	58.7	2130	1790
*193	89.84	11.230	4.50	97.0	50.0
$N_2^+ + H_2 \rightarrow N_2H^+ + H$					
194	34.89	2.326	1220×10^3	-	-
*195	84.32	5.621	114	2530	2600
196	70.09	4.673	132	3450	4400
197	110.23	7.349	29.5	950	820
198	133.86	8.924	11.2	590	335
*199	47.00	3.133	450	13000	28000
*200	121.68	8.112	19.8	940	680
$N_2^+ + HD \rightarrow N_2D^+ + H$					
207a	44.84	4.339	111×10^3	6900	7530
208a	59.84	5.791	36.5	4200	1750
210a	74.91	7.249	7.53	1100	358
211a	89.86	8.697	2.48	520	100
212a	105.36	10.197	0.72	188	42.3
213a	119.46	11.560	0.27	98	16
214a	35.05	3.392	160	-	-
$N_2^+ + HD \rightarrow N_2H^+ + D$					
207b	44.84	4.339	513×10^3	1570	1360
208b	59.84	5.791	323	720	538
210b	74.91	7.249	174	330	270
211b	89.96	8.697	53.5	183	188
212b	105.36	10.197	14.9	87	98
213b	119.46	11.560	8.0	50	58
214b	35.05	3.392	413	2700	2700

* Contour map of product distribution determined

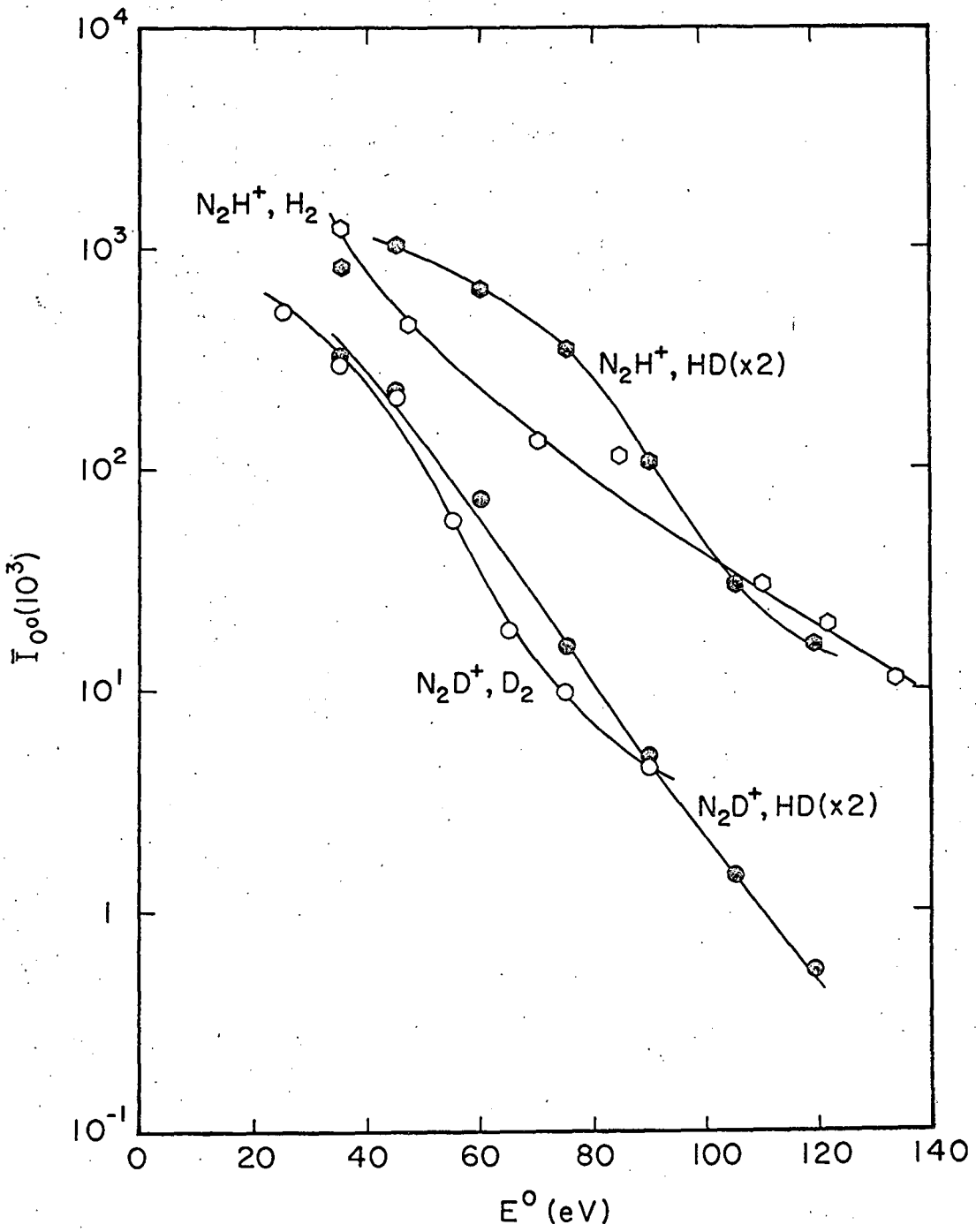

XBL 678-4794

Fig. 13 Log I_0o vs. E_i for $N_2^+ + H_2$, HD, D_2 reactions.

○ N_2D^+, D_2
⬡ N_2H^+, H_2
● N_2D^+, HD (x2)
⬢ N_2H^+, HD (x2)

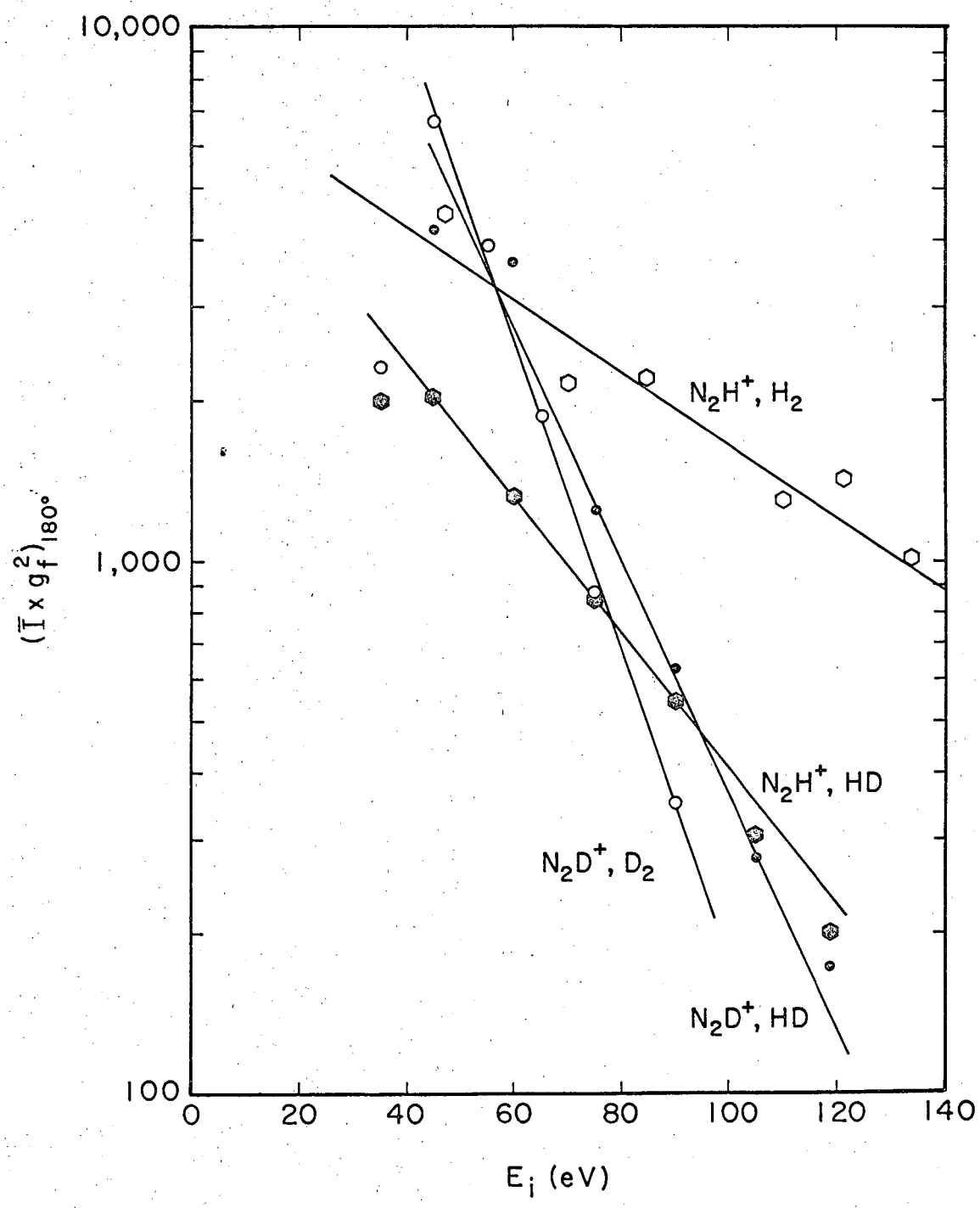

XBL 678-4788

Fig. 14 Log $(\bar{I}xg_f^2)_{180°}$ vs. E_i for $N_2^+ + H_2$, HD, D_2 reactions

○ N_2D^+, D_2
⬡ N_2H^+, H_2
◉ N_2D^+, HD
⬢ N_2H^+, HD

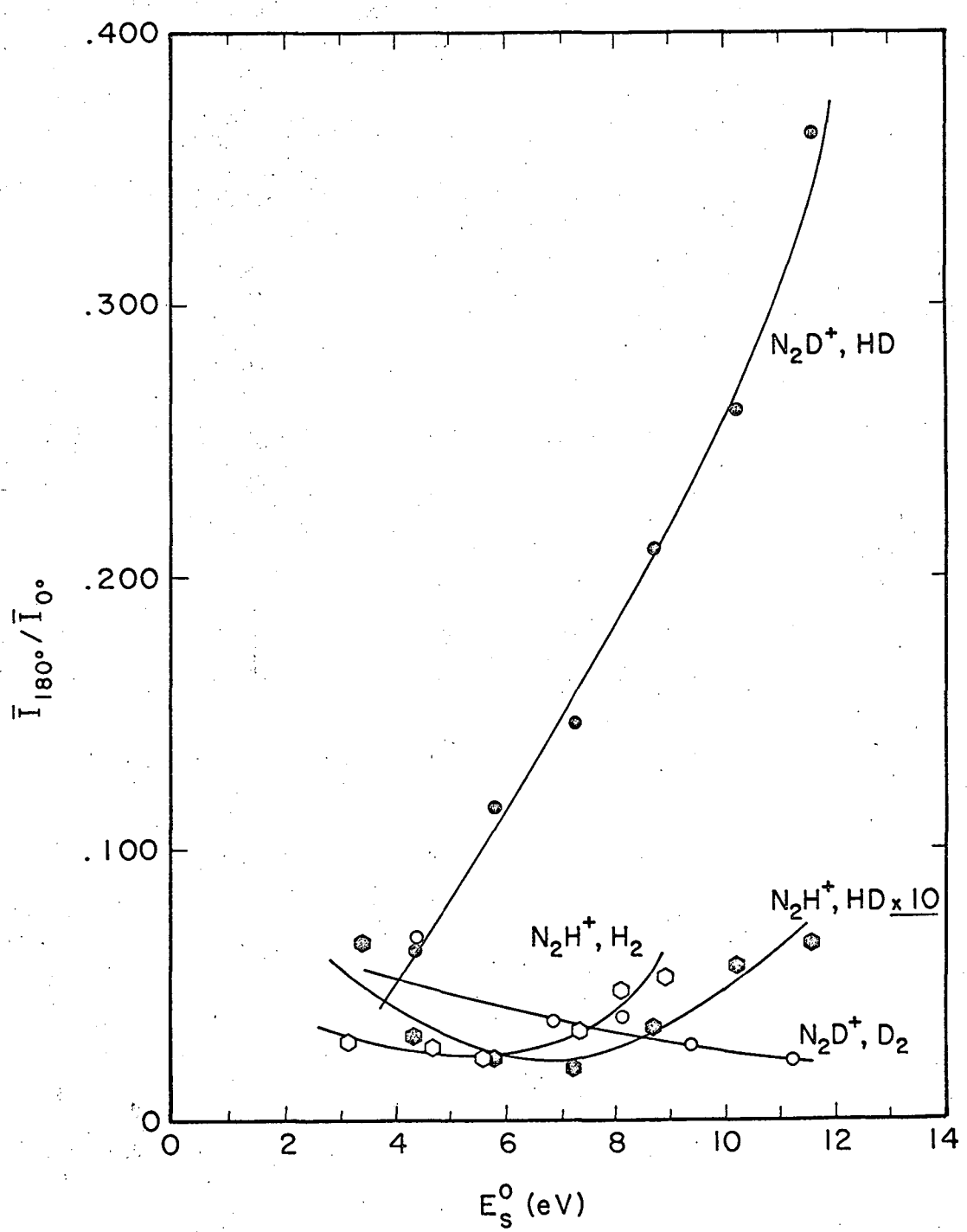

XBL 678-4787

Fig. 15 $\bar{I}_{180°}/\bar{I}_{0°}$ vs. initial relative kinetic energy for $N_2^+ + H_2$, HD, D_2 reactions. ○ N_2D^+, D_2; ⬡ N_2H^+, H_2; ◉ N_2D^+, HD; ⬢ N_2H^+, HD .

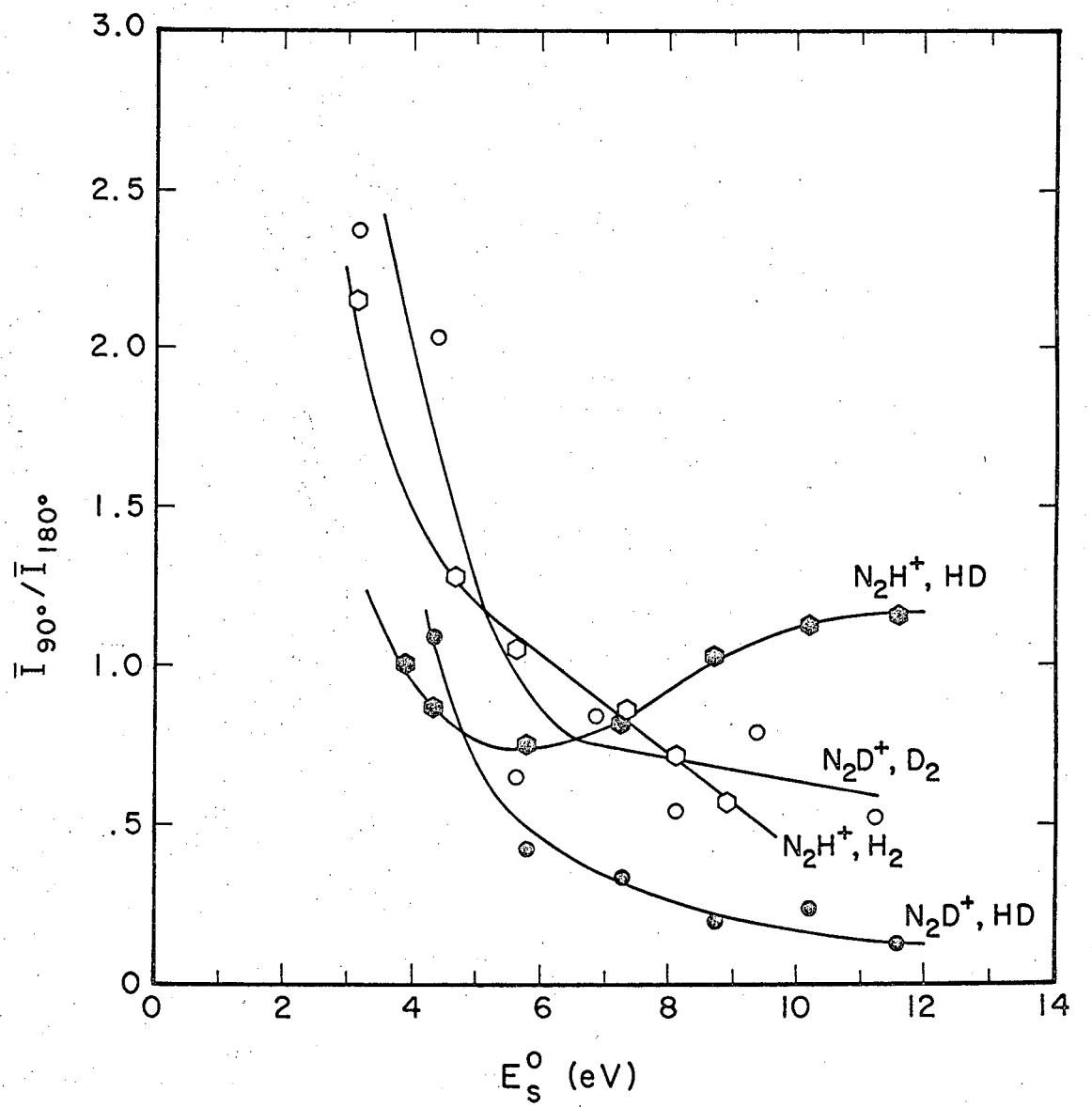

XBL 678-4786

Fig. 16 $\bar{I}_{90°}/\bar{I}_{180°}$ vs. initial relative kinetic energy for $N_2^+ + H_2$, HD, D_2 reactions.

○ N_2D^+, D_2

⬡ N_2H^+, H_2

● N_2D^+, HD

⬢ N_2H^+, HD

IV. Discussion and Interpretation

A. The Potential Energy Surface for the Reaction

The potential energy in a system consisting of a hydrogen molecule and an approaching N_2^+ ion is presumably fixed by the parameters shown in Fig. 17. With complete knowledge of the potential energy as a function of these six parameters it would in principle be possible to calculate from the initial conditions (impact parameter and rotational and vibrational phases) the trajectory of the ion through the collision and obtain the differential cross section. Computer tehcnology is at present far from being adequate for such a problem, however, the calculations having been only very recently extended to three-dimensional studies of certain simple cases of the reaction $A + BC \rightarrow AB + C$.[23,24] In view of the great similarity between the N_2^+ and Ar^+ reactions with isotopic hydrogen molecules[20,21,22] it would probably be an adequate first approximation to assume an averaged central potential for the N_2^+ ion, eliminating the parameters α_N, β and r_{N-N} and bringing the problem within range of Monte-Carlo calculations. At large separations r_s one can reasonably assume a potential due to the charge-induced dipole attraction of the form

$$V(r_s) = -\frac{e^2}{2}\alpha \; r_s^{-4} \qquad (17)$$

where α is the dipole polarizability of the H_2 molecule before the reaction and of the H atom after the reaction. Also, at large separations the fact that the reaction is exothermic requires that the N-H potential well be deeper than that of the hydrogen molecule. In the critical region of small r_s, however, almost nothing is known about the form of the potential energy surface except that from the temperature dependence of the

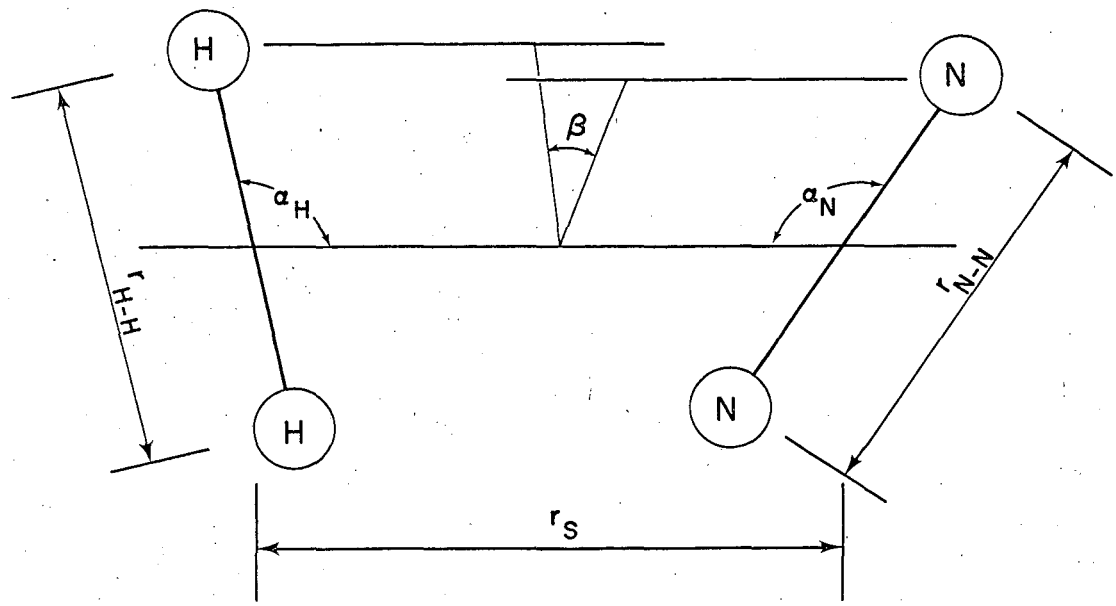

XBL 678-4798

Fig. 17 Parameters fixing the relative orientation of N_2^+ and H_2.

thermal energy rate constant there apparently is no activation energy barrier for the reaction.[2] Until detailed analysis is made of the dependence of the differential cross section on the shape of the potential energy surface it appears that the dynamics can be best understood through comparison with various simple models for the collisions.

B. Models for the Dynamics

1. Polarization Model

The most useful model for the interpretation of mass spectrometric data on ion-molecule reaction rates has been the polarization model proposed by Gioumousis and Stevenson.[25] In this model the attractive potential for the ion-induced dipole, given by Eq. (17) is assumed to govern the trajectory.

If classical mechanics holds the result is obtained that for a given relative velocity the collisions may be classified in two categories: particles having an impact parameter greater than a critical value b_o will never approach closer than a distance of $b_o/\sqrt{2}$, while those with impact parameters smaller than b_o will spiral to within an arbitrarily small distance of each other (assuming point particles). If it is assumed that reactions occur if and only if the distance between the particles is less than a critical value r_c which is less than $b_o/\sqrt{2}$ the total cross section is simply πb_o^2, which is found to be proportional to $E_s^{o-1/2}$. The differential cross section is determined by the unspecified details of atom transfer, but because of the large deflection angles undergone by particles involved in collisions with impact parameters near b_o the differential cross section cannot vary rapidly with angle.

Clearly for this model to be justifiable the orbiting cross section must be much greater than the gas kinetic cross sections of the particles. Only for very low (near thermal) energies is this criterion met. The detailed calculations of Herman et al.,[22] in fact, show the relatively weak polarization potential to have almost no influence on the trajectory in $N_2^+ + D_2$ reactions at laboratory energies higher than 20 eV.

2. Complex Model

The concept of an "activated complex" intermediate between reactants and products in a chemical reaction has been in vogue for a sufficiently long time that many chemists naturally expected to find from molecular beam experiments evidence for the existence of a long-lived collision complex. Such expectations, actually based on a misinterpretation of the requirements of transition state theory, have so far gone largely unfulfilled.

If a complex is formed which exists for several rotational periods the complex will essentially "forget" the details of how it was formed, except

for the requirements of the conservation laws. One would therefore expect to find an equal probability of dissociation of the complex at any CM angle in the plane of the collision. Because in collisions of a molecular beam with stationary target molecules the initial orbital angular momentum vectors always lie in a plane perpendicular to the beam direction, the distribution of products from the complex model will not be isotropic in three dimensions, but will show peaking at 0° and 180° in the CM system -- along the line where all the collision planes intersect.[27] The amount of peaking will be determined by the ratio of orbital angular momentum to the initially random rotational angular momentum. In any case the distribution must be symmetric about $X = 90°$ -- the plane of the initial orbital angular momenta. Such symmetry has been found only in alkali metal atom exchange reactions with alkali halides,[27] whereas in all other thermal energy alkali metal experiments[6] as well as for the ion-molecule reactions for which such information is known the differential cross sections show marked asymmetry about $X = 90°$. Even at relative kinetic energies as low as 0.1 eV the distribution of products from the $N_2^+ + D_2$ reaction is shifted far forward of the center of mass despite the relatively long range r^{-4} potential.[22] Angular asymmetry does not, of course, preclude the possibility of vibrational equilibration during the collision taking place within a time much shorter than a rotational period. Indeed, several vibrations of the reactants must occur while the interaction is still relatively strong, since even a 90 eV N_2^+ ion moves only 2Å during a vibrational period of H_2. Whether transfers of vibrational energy during a collision justify the use of the term "collision complex" is perhaps a moot point.

3. Stripping Model

The term "stripping collision" is derived from a not-quite-perfect analogy with the terminology of nuclear reactions and refers here to a

chemical reaction mechanism by which an atom of the neutral molecule is transferred to the ion without alteration of the original momentum vector of the remainder of the neutral. The stripping mechanism necessarily gives forward scattering in the CM system such as is observed in alkali metal reactions with Br_2[7] as well as the hydrogen atom transfer reactions of the present study. While making definite quantitative predictions about the energetics, the model also predicts some qualitative features of the intensity distribution.

Ideal Stationary Target Case

The predictions of the stripping model for zero target velocity are particularly straightforward. The completely inelastic collision of the ion with the transferred atom of mass $m_a = M_f - M_i$ gives by conservation of momentum

$$v_f = \frac{M_i}{M_f} v_i \tag{18}$$

and

$$E_f = \frac{M_i}{M_f} E_i \tag{19}$$

This gives for the final relative kinetic energy

$$E_s = \frac{m_f}{M_f + m_f} E_f = \frac{M_i m_f}{M_f m_i} E_s^o \tag{20}$$

and predicts a total kinetic to internal energy transfer

$$Q = - \frac{m_a}{M_f} E_i = - E_a^o \tag{21}$$

where E_a^o is simply the initial relative kinetic energy between the incident ion and the atom which is to be transferred.

It seems highly unlikely that a product ion with internal energy greater than its dissociation energy D will exist for a long enough time ($\sim 10^{-6}$ sec or $\sim 10^8$ vibrations) to be registered at the detector. There is therefore a maximum (negative) value of Q in a reaction which can lead to stable products.

Under the assumption that no internal energy exists in the hydrogen atom left over from the reaction this value is obtained from Eq. (9) by setting $H_i = 0$ and $H_f = D$:

$$Q_{max} = W - D \tag{22}$$

Depending on whether the product ion dissociates to $N_2^+ + H$ or to $N_2 + H^+$, D may have either of the values $D(N_2^+ + H)$ or $D(N_2 + H^+)$ where

$$D(N_2 + H^+) = D(N_2^+ + H) - I_{N_2} + I_H \tag{23}$$

and where the I's are the indicated ionization potentials. Since $W = D(N_2^+ + H) - D_{H_2}$ the corresponding values of Q_{max} are

$$Q_{max}(N_2^+ + H) = - D_{H_2} = - 4.5 \text{ eV} \tag{24}$$

and

$$Q_{max}(N_2 + H^+) = - D_{H_2} + I_{N_2} - I_H = - 2.5 \text{ eV}. \tag{25}$$

(Note that both Q_{max} values are independent of the product ion dissociation energy.)

The stripping model predicts, then, by Eq. (21) that no product ions will be found for primary ion energies higher than a critical value E_c given by

$$E_c = - \frac{M_f}{m_a} Q_{max} . \tag{26}$$

Values of E_c for the two possible dissociation modes are given in Table III along with other stationary stripping model predictions.

Table III

Predictions of the Stationary Target Stripping Model

Reaction	$\frac{v_f}{v_i} = \frac{E_f}{E_i}$	$\frac{E_s}{E_s^o}$	$E_c(N_2^+ + H)$(eV)	$E_c(N_2 + H^+)$(eV)
$N_2^+ + H_2 \rightarrow N_2H^+ + H$	0.9655	0.483	131	73
$N_2^+ + HD \rightarrow N_2H^+ + D$	0.9655	0.644	131	73
$N_2^+ + HD \rightarrow N_2D^+ + H$	0.9333	0.311	68	38
$N_2^+ + D_2 \rightarrow N_2D^+ + D$	0.9333	0.467	68	38

It is also to be expected from the stripping model that the intensity should be the same for formation of a given product ion from any isotopic molecule at the same energy E_a^o, since the remaining atom does not participate in the collision.

Modification to Include Target Motion

As noted in the section on data analysis, the location of the product ion peaks in a scattering cell experiment are not affected by the isotropic distribution of target velocities only if the variation of the cross section is small over the distribution of relative velocities, i.e., if the average velocity of the neutrals which react to scatter particles into the detector is zero. According to the stripping model, however, the cross section must go to zero at a relative velocity g_{max} corresponding to an initial relative kinetic energy E_a^o which exceeds Q_{max}:

$$\frac{m_a M_i}{2\ M_f}\ g_{max}^2 = -\ Q_{max}\ . \qquad (27)$$

Thus, only atoms having a velocity vector $\underset{\sim}{u}_a$ lying within a distance g_{max} of $\underset{\sim}{v}_i$ in $\underset{\sim}{v}$ space can contribute to the product ion signal. The implications of this requirement are demonstrated in Fig. 18. If the distribution in atom velocities $\underset{\sim}{u}_a$ (only the velocity of the transferred atom is important in the stripping model) is given by the function $f(u_a)$ of characteristic width γ then for a primary ion velocity $v_i = g_{max} - \gamma$ almost the entire distribution can react by the stripping model to give stable products. As the primary ion velocity is raised above this value, an increasing fraction of the atoms is prevented from reacting by the stripping model and the average velocity of the atoms which can react is no longer zero but some positive value. Finally, for $v_i > g_{max} + \gamma$, only reactions with those few atoms translating very rapidly in the direction of the ion beam can lead to the observed products.

The distribution in molecular velocities is Gaussian:

$$h(u_i) = \frac{dN}{d^3\underset{\sim}{u}_i} \propto e^{-u_i^2/\alpha^2} \tag{28}$$

where

$$\alpha = \sqrt{2kT/m_i} \tag{29}$$

is the characteristic width of the distribution, equal to the distance from $u_i = 0$ at which $h(u_i)$ decays to $1/e$ of its peak value. α is also equal to the most probable speed of the neutral molecules. If the atom transfer is regarded as instantaneous then the velocity distribution which is desired must include the vibrational motion of the atoms, since the transfer may take place at any phase of the neutral molecule oscillation. (The rotational velocity of the neutral is much less than the vibrational velocity and is therefore ignored.) The vibrational velocity distribution

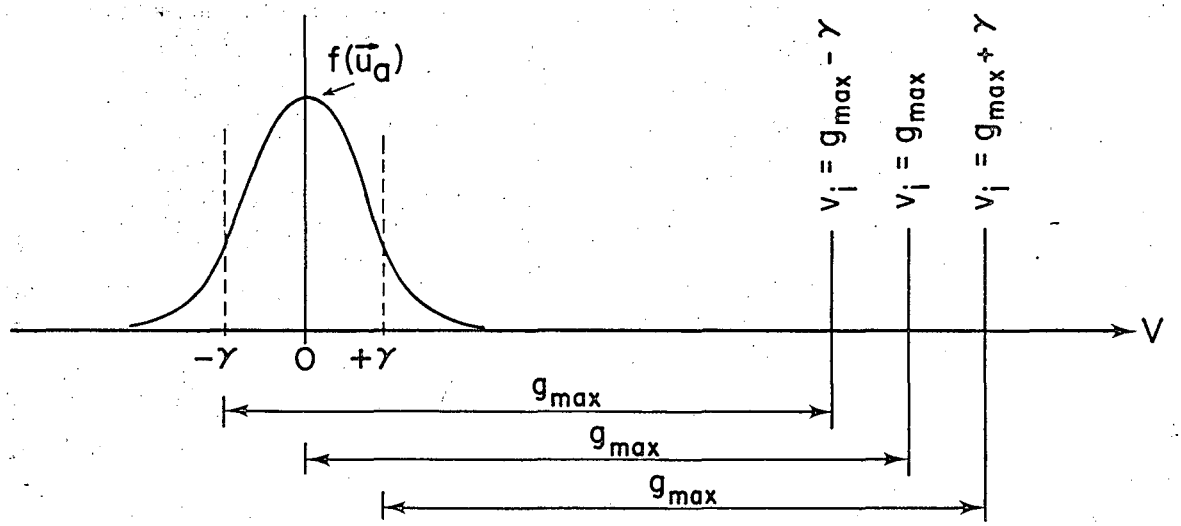

XBL 678-4797

Fig. 18 Influence of the target atom velocity distribution on the effective population for stripping model collisions.

for a ground-state harmonic oscillator is given by

$$j(u_g) = \frac{dN}{d^3 \underset{\sim}{u}_g} \propto e^{-(\mu/\hbar\omega)\, u_g^2} \tag{30}$$

where $\underset{\sim}{\mu}_g$ is the relative velocity of the two atoms. Since the vibrational velocity of the atom to be transferred is

$$u_v = \frac{m_f}{m_f}\, u_g \,, \quad \text{the} \tag{31}$$

distribution of atom velocities due to vibration is

$$j(u_v) \propto e^{-u_v^2/\beta^2} \tag{32}$$

where

$$\beta^2 = \frac{m_f}{m_a m_i}\, \hbar\omega \quad . \tag{33}$$

The desired distribution $f(u_a)$ in atom velocities is then just the convolution of translational and vibrational distributions, given by

$$f(u_a) = h(u_i)*j(u_v) \propto e^{-u_a^2/\gamma^2}, \tag{34}$$

which is a Gaussian function with width parameter

$$\gamma = \sqrt{\alpha^2 + \beta^2} \quad . \tag{35}$$

At energies much above the critical energy E_c only target atoms moving on the average in the same direction as the ion beam can react to give stable products. The stripping model prediction for the product velocity is then

$$v_f = \frac{M_i}{M_f} v_i + \frac{m_a}{M_f} u_a \quad . \tag{36}$$

But since the population of target atoms decreases rapidly with increasing velocity and reactions can be observed only for $u_a \geq v_i - g_{max}$, the average velocity of the neutrals leading to reaction is approximately

$$u_a = v_i - g_{max} \quad . \tag{37}$$

Substitution into Eq. (36) gives

$$v_i - v_f = \frac{m_a}{M_f} g_{max} \tag{38}$$

which should be valid for ion energies above E_c. By the same token, at high energies the relative velocity of reacting particles is always $\sim g_{max}$, so the cross section is constant and the intensity should be directly proportional to the effective population of target atoms,

$f(v_i - g_{max})$. The stripping model requirement for the high energy variation of the intensity is therefore

$$\ell n\bar{I} = -\frac{1}{\gamma^2}(v_i - g_{max})^2 + \text{constant} \qquad (39)$$

$$\frac{d\ \ell n\bar{I}}{d\ E_i} = -A + BE_i^{-1/2} \qquad (40)$$

where $A = 2/M_i\gamma^2$ and $B = (2/\gamma^2)\sqrt{2/M_i}\ g_{max}$.

The effects of target motion on the stripping model predictions are summarized in Table IV. The slope of log $\bar{I}$ vs. E_i is evaluated at the energy

$$E_m = \frac{1}{2} M_i (g_{max} + \gamma)^2$$

at which the modified stripping model should become valid.

Error in Q Due to Target Motion

Both E_s^o and E_s are calculated assuming the average velocity of the target molecules to be zero. If, as in the modified stripping model, at some energies the average velocity of molecules leading to the observed products is not zero, then an error will be made in both E_s^o and E_s. Since the errors are both in the same direction for forward scattering from molecules moving parallel to the primary beam, part of the error cancels in Q. For the stripping model all of the error first order in u_i cancels, leaving

$$Q_{error} = Q_{app} - Q_{real} = \frac{m_i m_a}{2\ m_f}\ u_i^2 . \qquad (41)$$

Table IV

Predictions of the Modified Stripping Model

Reaction	α (10^5 cm/sec)	β (10^5 cm/sec) *	γ (10^5 cm/sec)	g_{max} (10^5 cm/sec) †	$(v_i - v_f)$ (10^5 cm/sec)	$-(d \log I/dE_i)_{E_m}$ (eV^{-1})
$N_2^+ + H_2 \rightarrow N_2H^+ + H$	1.58	2.03	2.57	22.4	0.77	0.66 at 90.6 eV
$N_2^+ + HD \rightarrow N_2H^+ + D$	1.29	2.19	2.54	22.4	0.77	0.67 at 89.8 eV
$N_2^+ + HD \rightarrow N_2D^+ + H$	1.29	1.09	1.69	16.1	1.07	0.77 at 45.9 eV
$N_2^+ + D_2 \rightarrow N_2D^+ + D$	1.12	1.21	1.65	16.1	1.07	0.74 at 45.9 eV

* Frequency data taken from Herzberg.[26]

† Calculated for $Q_{max} = -2.5$ eV.

Only the translational velocity of the target molecule causes an error, because the relative kinetic energy is defined with respect to the center of mass of the neutral. The error from Eq. (41) is less than the experimental scatter (~0.5 eV) in measurements of Q for $u_i < 3$ to 6α, depending on the isotope.

4. The Rebound Mechanism

The opposite case to the stripping mechanism is a process in which reaction occurs only for small impact parameter "head-on" collisions of the reactants, which necessarily scatter the ion backward in the CM system. Preferential backward scattering of the alkali halide product has been observed in alkali metal atom reactions with CH_3I.[7] It is not possible to predict the energetics of such collisions without hypothesizing the nature of the (at least) three-body interaction.

C. Comparison of the Experimental Results with the Models

Although the large- and small-angle scattering processes must be related in the sense that they both arise from motion of the particles along the same potential energy surface, the features are rather sharply separated in the resolved contour maps and show little direct connection between the respective energetic and intensity data. They are therefore discussed separately.

1. Forward Scattering

The most prominent feature of the product ion distributions is the peak at 0° in the CM system, which has an intensity between 3 and 500 times that for large-angle scattering. Throughout the energy range covered in these experiments the half-maximum width of the 0° product ion peak in the LAB system showslittle or no spreading in energy or angle over the dimensions of the primary beam. This fact implies that the collisions responsible for the 0° peak are "weak", i.e., that the interaction of the ion with the leftover atom of the neutral is not strong enough to cause a large deflection. Rebound of the particles from the strong repulsive part of the potential, necessarily resulting mostly in large-angle scattering, can be avoided only if the impact parameters of the collisions are sufficiently large ($> \sim 2\text{Å}$). This observation, coupled with the fact that the absolute value of the cross section for small angle scattering varies from about 20Å^2 at the lowest relative kinetic energies to less than $0.1\ \text{Å}^2$ at the highest,[20] leads to the conclusion that the 0° peak results from large impact parameter collisions where the probability of atom transfer at a given impact parameter decreases rapidly with increasing energy. A strong dependence of the transfer probability on the relative orientation or vibrational phases of the reactants, with the range leading to reaction a decreasing function of energy, would provide a mechanistic explanation for this phenomenon. Since the strong forward peaking is predicted by the stripping model, further comparison is warranted.

In Fig. 19 a plot of final versus initial relative kinetic energy for 0° scattering is given. It is seen that the data for all the isotopes satisfactorily follow the predictions of the stationary target stripping model (taken from Table III) out to energies where Q becomes approximately -2.5 eV, and at high energies fall near the Q = -2.5 eV line, consistent with the modified stripping model. These features were observed for the $N_2^+ + D_2$ reaction by Doverspike, et al.,[21] and were reflected in the shift of the product ion velocity spectra to higher values than predicted by the stationary target stripping model, as first observed by Lacmann and Henglein.[20] The -2.5 eV limiting value of Q suggests strongly that the principal products of the N_2H^+ dissociation are $N_2 + H^+$, though smaller amounts of dissociation to $N_2^+ + H$ are not precluded.

Another prediction of the stripping model is that the cross section for formation of a given product ion should depend only on E_a^o, not on the nature of the remaining atom in the target molecule. The calculations of the differential cross sections $\bar{I}$ include the factor $V_{EA}^{3/2}$ used to normalize the data to the same detector volume element in $\underset{\sim}{v}$ space. This gives a value which will be equal to the true differential cross section if the distribution varies slowly within the limits of the detector volume. For a product ion peak of the same shape as the primary beam peak, however, the true cross section is simply the ratio of peak intensities. The total cross section for 0° scattering thus calculated by omitting the $V_{EA}^{3/2}$ factor in $\bar{I}_{0°}$ are plotted versus E_a^o in Fig. 20. Within the scatter, which at low energies is rather large, the data for both N_2H^+ and N_2D^+ products appear to fall on a straight line corresponding to the relation

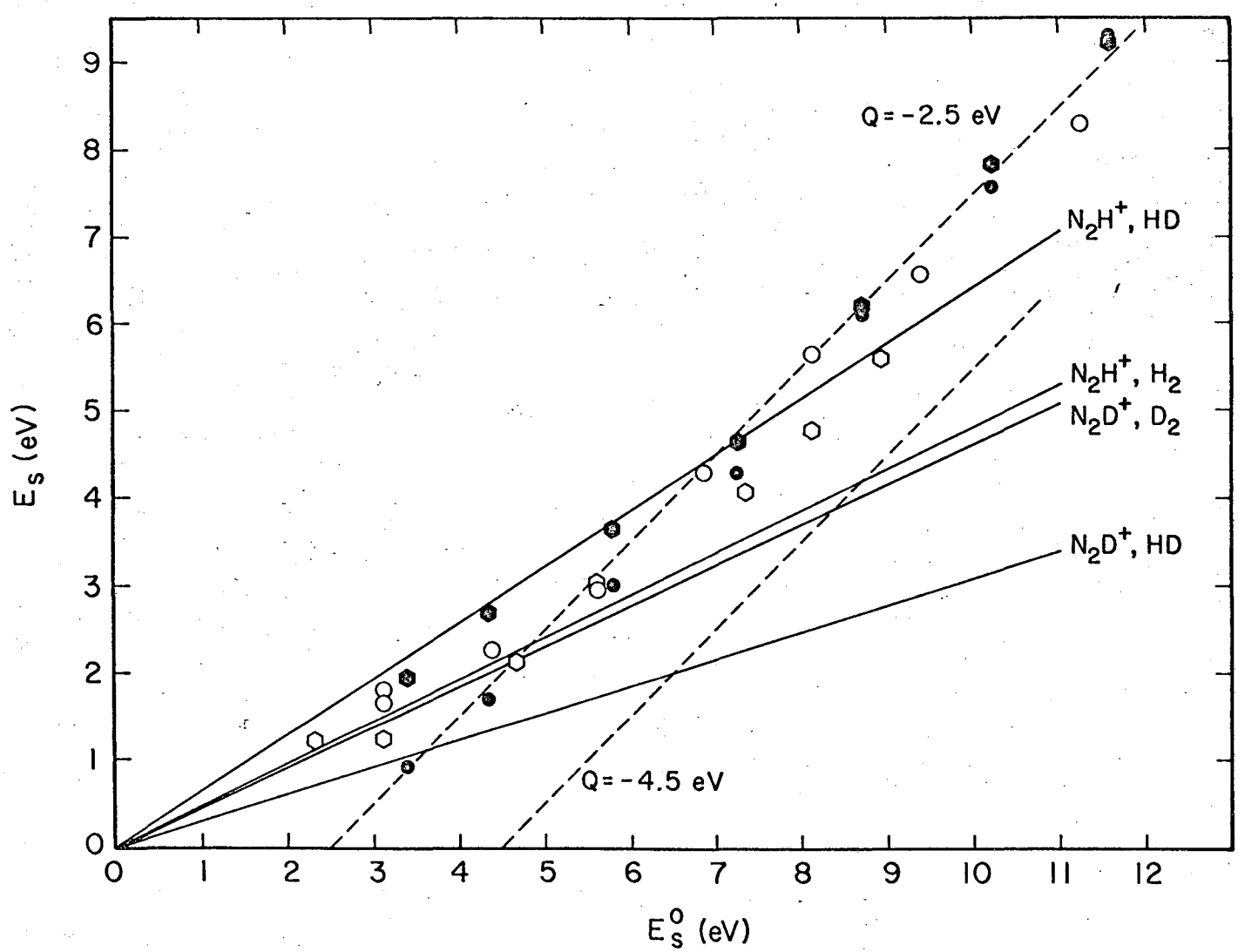

XBL 678-4793

Fig. 19 Final vs. initial relative kinetic energy for 0° scattering.
○ N_2D^+, D_2; ⬡ N_2H^+, H_2; ◉ N_2D^+, HD; ⬢ N_2H^+, HD

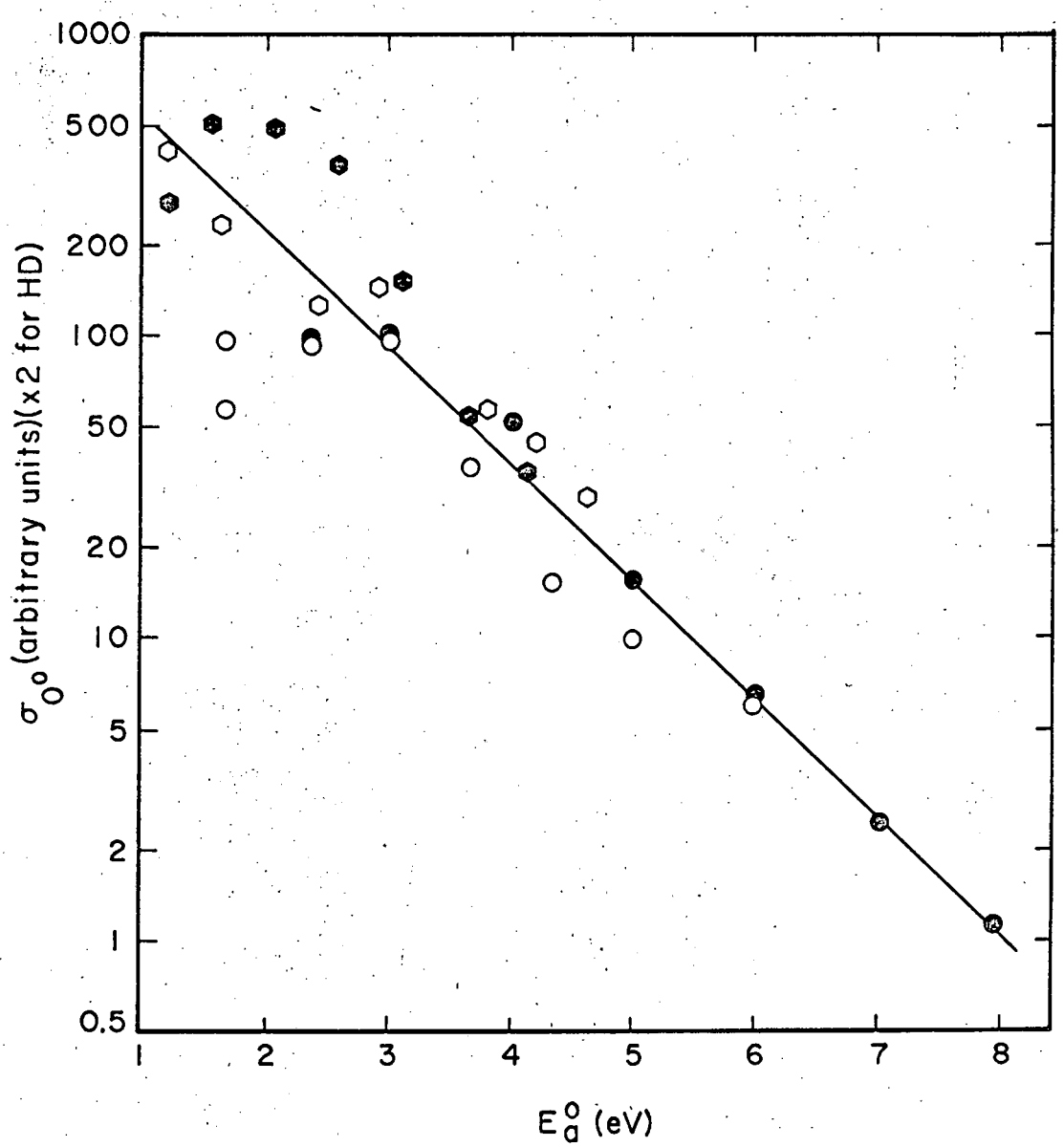

XBL 678-4783

Fig. 20 Total cross section for 0° scattering vs. initial atom relative kinetic energy E_a^0.

○ N_2D^+, D_2
⬡ N_2H^+, H_2
● N_2D^+, HD (x2)
⬢ N_2H^+, HD (x2)

$$\log \sigma_{o^\circ} = -0.39\ E_a^o + \text{constant}\ .$$

The slope agrees very well with the value $-0.36\ eV^{-1}$ measured from the data of Lacmann and Henglein for the H_2 and D_2 reactions.

It is obvious from Fig. 13 that the small angle scattering cross sections do not go to zero at the values of E_c given in Table III for $Q = -2.5$ eV. Despite the several features of the data which seem to be adequately predicted, the stripping model can be valid at high energies only if the distribution in target atom velocities is sufficient to explain the variation in intensity. Comparison of the data in Fig. 13 with the slopes given in Table IV clearly show this not to be the case. There are no observable breaks in the plots of log $\overline{I}$ vs. E_i at energies corresponding to $v_i = g_{max}$, and the experimental slopes are about a factor of 20 less negative than those predicted by the falloff of target atom population with velocity. The number of target atoms in the necessary velocity range is thus far from sufficient to give the observed intensities from stripping model collisions. While it is not guaranteed by this observation that the average velocity of target atoms leading to the observed reactions is zero after all, the average must be much closer to zero than a few γ. For a high energy collision with a slow molecule to result in forward scattering with only -2.5 eV energy defect it is kinematically necessary for the remaining atom to be kicked backward in the LAB coordinate system. As an example, consider the point of highest E_a^o in Fig. 20. The stationary target stripping model, in which the leftover atom remains stationary in the LAB system, predicts a Q value of $Q_{SM} = -8.0$ eV and a final relative kinetic energy of 3.6 eV. To obtain a stable product,

however, (Q_{max} = -2.5 eV) there must be 5.5 eV less of the initial relative kinetic energy converted to excitation energy. This amount must therefore appear as additional kinetic energy of the products and can only arise from backward recoil of the remaining H atom. The recoil energy (defined here as $Q_{max} - Q_{SM}$) can be lowered somewhat from the apparent value if reactions occur preferentially with target molecules moving in the same direction as the primary ions.

There is some degree of difficulty in reconciling the kinematic requirements of strong recoil with product ion scattering peaked very near $\chi = 0°$. For such scattering to occur it is necessary for the incident ion to move past the target molecule with little angular deflection, pick up one of the atoms, then push the other atom rapidly back toward the ion beam origin. To answer the question of why there is not a wide distribution of angles backward in the LAB system into which the H atom recoils, it helps to note that the experimental observations do not show that such processes do not occur, but only that they do not lead to stable products. A mechanism might be envisioned which requires for small angle scattering that the orientation of the target molecule be parallel to the incident ion velocity vector and that the phase of the oscillation be such that electronic rearrangement during the collision leaves the leftover atom on a strong repulsive potential wall. For other orientations and vibrational phases the recoil would not be strong enough to stabilize the product ion in this purely speculative mechanism.

2. Large-angle Scattering

A mechanistic interpretation of the large angle scattering data is much more difficult than the description of small angle scattering. An intensity which varies little with scattering angle is predicted not only by a complex model for the reaction, but is in general a property of "head-on" impulsive collisions where the particles rebound from strong repulsive potentials. The elastic collision of hard spheres, for example, gives isotropic scattering in the CM system. The fact that the final relative velocity seems to be independent of the scattering angle is more strongly suggestive of a long-lived complex mechanism, yet it is also possible to explain such behavior on the basis of purely impulsive collisions.

Figure 21 shows a plot of final vs. initial relative kinetic energy for all the data where the large angle scattering is resolved. With the exception of the highest energy points for the N_2D^+ product from HD all the data fit close to the straight line shown for Q = -1.75 eV. This value is significantly lower than the Q values for 0° scattering. While the lower product ion internal energy implied by this observation is consistent with the fact that a strong collision allows more opportunity for imparting large translational energy to the leftover atom, the constant -1.75 eV value of Q is puzzling in view of the rapidly decreasing intensity as a function of energy. A low intensity at the CM point in the contour maps is required at high primary ion energies by the dissociation of product ions having low final relative kinetic energies and hence large excitation energies. That such dissociation is not solely responsible for the crater-like shapes of the distributions, however, is indicated by a Q value less than that required for dissociation. Impulsive collision

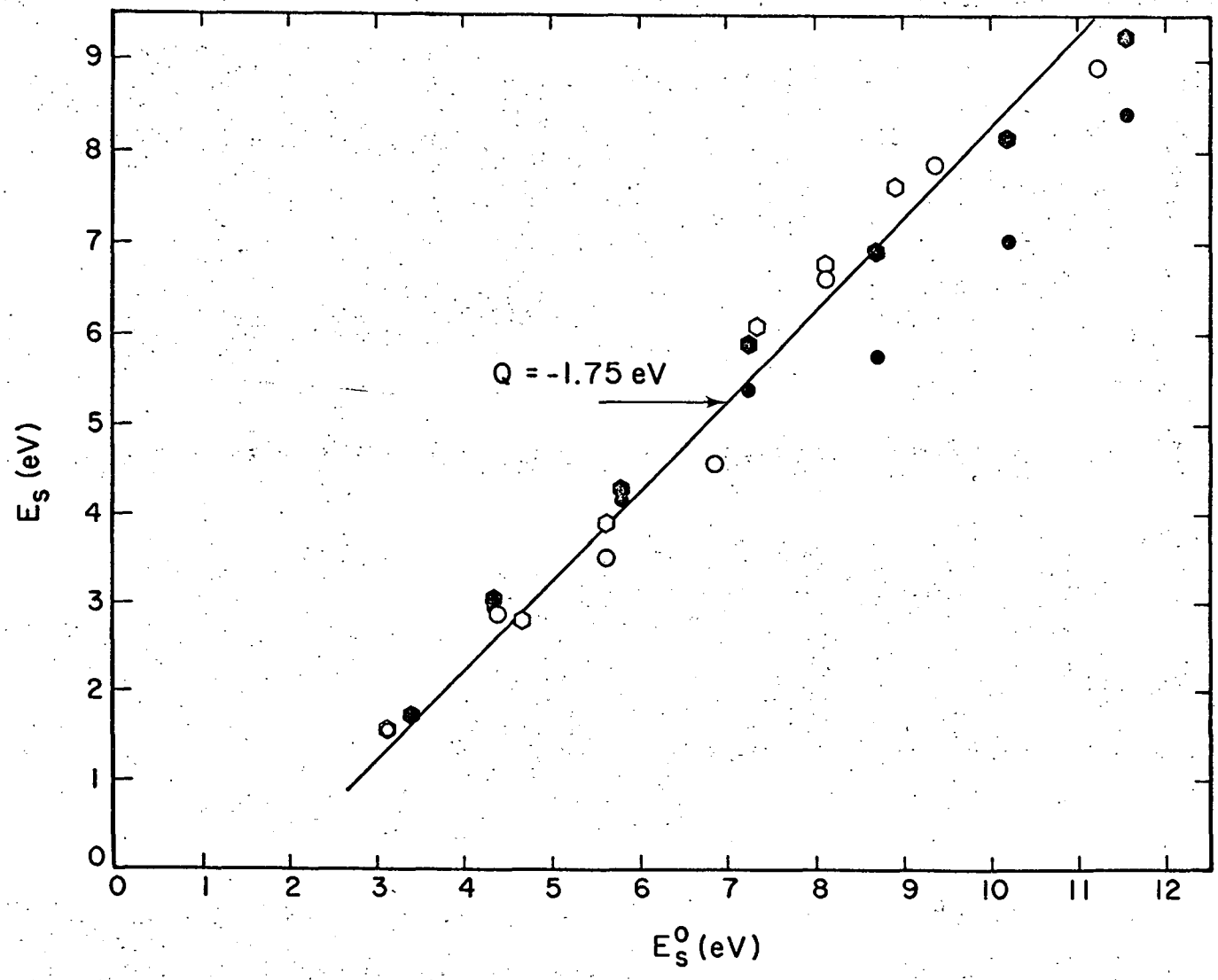

XBL 678-4792

Fig. 21 Final vs. initial relative kinetic energy for large-angle scattering.
○ N_2D^+, D_2; ⬡ N_2H^+, H_2; ◉ N_2D^+, HD; ⬢ N_2H^+, HD

models such as, for example, a head-on completely inelastic collision of the ion with the first target atom encountered followed by an elastic collision of the product ion with the remaining target atom, would be expected to give fairly isotropic angular distributions, but would lead to predictions of increasing product ion excitation as the collision energy is increased.

Large isotope effects are evident in the energy variation of the backward scattering cross sections as shown in Fig. 14. Except for a vague similarity in slope for the reactions to form a given product, however, no correlation is evident. The peaking at 180° shows particularly interesting, though likewise inexplicable, isotope effects. At 180° the high energy reactions with HD yield approximately the same intensities of N_2H^+ and N_2D^+ products. The cross section for N_2D^+ formation falls off drastically at smaller CM scattering angles, while that for N_2H^+ increases. It might be pointed out that the stronger peaking in the backward direction with increasing energy, observed for all the reactions except the reaction with HD to form N_2H^+, is consistent with a complex model in which the average dissociation time for the complex is comparable to half a rotational period at low energies but becomes much shorter than a rotational period at high energies, or alternatively, an impulsive collision model which requires more nearly "head-on" collisions to give stable products as the energy is increased. There is no apparent reason why the $N_2^+ + HD \rightarrow N_2H^+ + D$ reaction should deviate from the others in this respect, however.

V. Conclusions

The experiments reported here show in great detail the features of the complete product energy and angular distributions for the $N_2^+ + H_2$, HD, D_2 reactions. While certain individual features of the distributions seem to correlate with simple collision models, the combination of such large quantities of energetic, intensity and isotope effect data provides much too stringent a test for any simple model to meet successfully. For example, though the stripping model predicts at all energies the angular distribution features of the 0° peak, the high energy data clearly show recoil of the product ion to occur, and the lack of any transition in the intensity at energies around E_c suggests that even the low energy agreement of the energetics with the stripping model may be accidental. Similarly, some of the large-angle scattering data can be more satisfactorily interpreted in terms of a long-lived collision complex than by impulsive rebound collisions despite the strong intuitive notion that such a weakly bound complex cannot survive more than a few vibrations at the highest relative kinetic energies used in these experiments.

It must be concluded that much additional theoretical study is necessary before these reactions can be said to be "understood". Through Monte-Carlo calculations of the differential cross sections for various potential forms, the wealth of correlated data for these reactions should provide an excellent opportunity for investigating the short range features of the potential energy surface for reaction. Rigid tests of theories for special cases, such as the atom transfer probability at large impact parameters or in head-on linear collisions are also possible.

Experimentally, it would be valuable to have the same isotope effect and large-angle scattering data on reactions with CO^+ to investigate influences due to the similarity of N_2 and H_2 ionization potentials (15.8 eV for N_2 and 15.43 eV for H_2) which could affect the potential energy surface by permitting charge-transfer at fairly large intermolecular distances, and on reactions with Ar^+ to study the differences (if any) between reactions with diatomic and monatomic ions. Also of great interest are data on channels for the collision products other than formation of stable N_2H^+ or N_2D^+ ions. Studies of this type have recently been begun in this laboratory and are expected to yield important correlations with the reactive scattering data.

REFERENCES

1. Excellent recent reviews on the investigation of ion-molecule reactions with conventional and tandem mass spectrometers have been given by Talroze[2] and Stevenson.[3]
2. V. L. Talroze, Pure and Appl. Chem. 5, 455 (1962).
3. D. P. Stevenson, "Ion-Molecule Reactions," Chapter 13 in Mass Spectrometry, C. A. McDowell, Ed. (McGraw-Hill, New York, 1963).
4. A. A. Frost and R. G. Pearson, Kinetics and Mechanism, (John Wiley and Sons, New York, 1961), p. 77.
5. A complete bibliography of molecular beam studies of chemical reactions up to 1964 has been given by Herschbach,[6] who also reviewed the subject in 1966.[7] For discussions of the kinematic analysis in molecular beam experiments, see articles by Morse and Bernstein,[8] who treat the general conversion from laboratory to CM coordinates, and by Herschbach.[9]
6. D. R. Herschbach, Appl. Optics Supplement on Chemical Lasers (1965), pp. 142-143 contain a complete bibliography on molecular beam experiments and theoretical analysis up to 1964.
7. D. R. Herschbach, "Reactive Scattering in Molecular Beams," Ch. 9 in Molecular Beams, John Ross, Ed. (Interscience, Div. of John Wiley and Sons, New York, 1966).
8. F. A. Morse and R. B. Bernstein, J. Chem. Phys. 37, 2019 (1962).
9. D. R. Herschbach, Disc. Faraday Soc. (1962), p. 149.
10. H. Pauly and J. P. Toennies, Adv. in Atomic and Molecular Physics, Vol. 1 (1965), p. 250 f.

11. R. R. Herm and D. R. Herschbach, J. Chem. Phys. 43, 2139 (1965).

12. P. R. Brooks and E. M. Jones, J. Chem. Phys. 45, 3449 (1962).

13. R. J. Beuhler, R. B. Bernstein and K. H. Kramer, J. Am. Chem. Soc. 88, 5331 (1966).

14. H. Gutbier, Z. Naturforsch. 12A, 499 (1957).

15. D. O. Schissler and D. P. Stevenson, J. Chem. Phys. 24, 926 (1956).

16. C. F. Giese and W. B. Maier, J. Chem. Phys. 39, 739 (1963).

17. B. R. Turner, M. A. Fineman and R. F. Stebbings, J. Chem. Phys. 42, 4088 (1965).

18. T. F. Moran and L. Friedman, J. Chem. Phys. 42, 2391 (1965).

19. See W. R. Gentry, University of California, Lawrence Radiation Laboratory Report UCRL-17691.

20. K. Lacmann and A. Henglein, Ber. Bunsenges. Physk. Chem. 69, 279-296 (1965).

21. L. D. Doverspike, R. L. Champion and T. L. Bailey, J. Chem. Phys. 45, 4385 (1966).

22. Z. Herman, J. D. Kerstetter, T. L. Rose and R. Wolfgang, J. Chem. Phys. 46, 2844 (1967).

23. D. L. Bunker and N. C. Blais, J. Chem. Phys. 41, 2377 (1964).

24. L. M. Raff and M. Karplus, J. Chem. Phys. 44, 1212 (1966).

25. G. Gioumousis and D. P. Stevenson, J. Chem. Phys. 29, 294 (1966).

26. G. Herzberg, Spectra of Diatomic Molecules, 2nd. Ed. (Van Nostrand, New York, 1950).

27. W. B. Miller, S. A. Safron and D. R. Herschbach, to be published in Discussions of the Faraday Society.

ACKNOWLEDGMENTS

It is a pleasure to acknowledge here the support and encouragement of my wife, Sharron, the many helpful discussions and ideas contributed by Dr. Bruce H. Mahan and Dr. Yuan-tseh Lee, and the aid in carrying out the experiments provided by Dr. Eric.A. Gislason, Mr. Chi-wing Tsao and Mr. Arthur Werner.

Three years of support from a National Science Foundation Graduate Fellowship are also gratefully acknowledged.

This work was done under the auspices of the United States Atomic Energy Commission.

This report was prepared as an account of Government sponsored work. Neither the United States, nor the Commission, nor any person acting on behalf of the Commission:

A. Makes any warranty or representation, expressed or implied, with respect to the accuracy, completeness, or usefulness of the information contained in this report, or that the use of any information, apparatus, method, or process disclosed in this report may not infringe privately owned rights; or

B. Assumes any liabilities with respect to the use of, or for damages resulting from the use of any information, apparatus, method, or process disclosed in this report.

As used in the above, "person acting on behalf of the Commission" includes any employee or contractor of the Commission, or employee of such contractor, to the extent that such employee or contractor of the Commission, or employee of such contractor prepares, disseminates, or provides access to, any information pursuant to his employment or contract with the Commission, or his employment with such contractor.